CONTACT MODELING FOR A NONLINEAR IMPACT OSCILLATOR

BY

RYAN E. CARTER

A THESIS PRESENTED TO THE GRADUATE SCHOOL
OF THE UNIVERSITY OF FLORIDA IN PARTIAL FULFILLMENT
OF THE REQUIREMENTS FOR THE DEGREE OF
MASTER OF SCIENCE
UNIVERSITY OF FLORIDA
2005

ACKNOWLEDGMENTS

I would like to thank the United States Air Force SEEK EAGLE Office and PALACE ACQUIRE sponsors for making this opportunity possible. Special thanks are due to my wife and family for their personal support, and to Dr. Brian Mann, Mike Koplow, Raul Zapata, and Jennifer Tate of the Nonlinear Dynamic Systems group for technical advice and assistance.

TABLE OF CONTENTS

LIST OF FIGURES

Abstract of Thesis Presented to the Graduate School
of the University of Florida in Partial Fulfillment of the
Requirements for the Master of Science

CONTACT MODELING FOR A NONLINEAR IMPACT OSCILLATOR

By

Ryan E. Carter

August 2005

Chair: Dr. Brian P. Mann
Major Department: Mechanical and Aerospace Engineering

Impact oscillators, or vibro-impact systems, have been used to study impacting behavior and nonlinear dynamics. These systems are representative of many real world systems which experience impacts or other types of motion limiting discontinuities, such as stick-slip arising from dry friction. This thesis presents an experimental investigation of a parametrically excited nonlinear impact oscillator with an emphasis on correctly modeling the observed nonlinear behavior. Approaches to modeling and analyzing an impact oscillator are presented, comparisons are made between experimental and theoretical results using several different contact models, and multiple types of interesting nonlinear behavior are demonstrated. This results in a deeper understanding of the methods available for contact modeling which provides a means of analyzing more complex impacting systems, achieving a higher fidelity prediction of the system response, and investigating new types of nonlinear behavior.

CHAPTER 1
INTRODUCTION

Discontinuous dynamical systems arise in many applications of every day life. These include areas of mechanical, aerospace, and marine engineering, the automotive industry, machining, and many other fields of testing, research, and engineering application. Although nonsmooth dynamical systems are common in application, a general and comprehensive approach to analyzing and modeling these systems does not exist. Difficulties arise from an incomplete understanding of the underlying physics, limitations of testing and measurement, and lack of the appropriate mathematical tools. For these reasons, the area of discontinuous dynamics remains a field where further research and development is needed.

Problems involving impact are a particularly interesting subset of discontinuous dynamical systems. Examples of this type of system include gearboxes, pivoting joints, mooring ships, motion limited devices such as shocks and struts, aircraft landing gear, machining tools and cutting devices, vibro-impact absorbers, sports such as baseball and tennis, and so on. In many instances, the impacts are intentional and necessary to accomplish the overall objective of the system. In other cases, the impacts are unwanted and may result in excessive vibration, passenger discomfort, or premature wear and failure. Regardless of the situation, it is often desirable to understand the physics governing the impact, develop one or more mathematical models, and design or modify the system to accomplish the desired effect.

Impact oscillators, also referred to as vibro-impact systems, are an intriguing application of impacting systems and have been shown to exhibit a wide range of interesting nonlinear behavior. These mechanical devices often consist of one or more parametrically excited rigid bodies with motion limiting stops. Even simplistic single degree of freedom systems have been shown to demonstrate complicated nonlinear behavior such as period doubling bifurcations, grazing bifurcations, and chaos [15,21-24,26,28,31]. Treatment of these systems is usually accomplished by selecting piecewise continuous mathematical models. When the oscillatory motion of the mechanical device between impacts is linear, an exact solution exists for free flight behavior [15]. When the motion is nonlinear, as in the case of a pendulum oscillating at arbitrarily large angles, the equations of motion do not admit an exact solution and numerical integration is often used [1].

Analysis of Low Speed Impact

Low speed impact is a subset of collision mechanics dealing with impact resulting in little or no permanent deformation, in contrast to a high speed impact, such as an automobile collision. Low speed impacts can be classified according to the alignment of the centers of mass and the geometrical form of the bodies involved in the collision. The alignment of the centers of mass is referred to as the *impact configuration*. When the centers of mass are aligned, as in the collision of two identical spheres, the impact is *collinear*, otherwise, the impact configuration is *eccentric*. The types of low speed impact models include particles, rigid bodies, and transverse or axial flexible bodies. Particles are massless bodies useful for modeling simplistic, ideal impacts. Rigid body models are by far the most common and can be used to model elastic and inelastic collisions.

Flexible bodies can be used to model impacts when significant vibrations far removed from the impact site are important.

Rigid Body Impacts

The level and complexity of the mathematical model necessary to accurately describe the collision of two or more rigid bodies is dependent on the impact configuration, material properties of each body, and relative velocity prior to impact. It should be noted that the term "rigid body" does not imply that deformation does not occur during impact. The rigid body assumption requires that the only deformation that occurs during impact be near the impact region. For instance, the rigid body assumption for a bowling ball colliding with bowling pins would be sufficient because the deformation of the bodies is minute and restricted to the region of contact. However, a tennis ball impacting a stiff racket may experience significant deformation, changing the shape of the entire body, negating the rigid body assumption.

For low speed impacts between two bodies, the *compliance* of the bodies gives rise to a very rapidly increasing reaction force during the *compression* phase that tends to slow the bodies to zero relative velocity. Subsequently, the reaction force declines as the bodies are forced apart during the *restitution* phase. The instant of zero relative velocity separating the compression and restitution phases is the point of maximum *penetration* or *approach*. In an *elastic* impact, the kinetic and potential energy components are perfect compliments and the total kinetic energy at *incidence* is precisely the same as the total kinetic energy at *separation*. In any physical situation, some non-frictional energy is dissipated during impact giving rise to an *inelastic* impact where the kinetic energy at separation is less than the kinetic energy at incidence. When the energy dissipation is rate dependent, or viscous, the impact is *viscoelastic*. Viscoelasticity is a material

property that is analogous to a viscous damper or dashpot in linear system theory. Viscoelasticity implies that the amount of energy dissipated during an impact will increase with increasing relative velocity.

When the impacting bodies are “hard”, or the motion of the bodies away from contact is large, the time *duration* of contact is assumed to be vanishingly small. For “soft” bodies, or when the motion of the bodies is on the same scale as the motion during contact, the contact duration becomes an important part of the system response. This difference has given rise to rigid body contact models for low speed impact including instantaneous and finite time approximations with varying degrees of complexity.

Additionally, the number of degrees of freedom (DOF) necessary to describe the motion during contact, i.e. the impact configuration, has a significant affect on the model complexity. For two or more DOF, friction and slipping may dominate the system response during impact necessitating more complicated models.

Thesis Content

The goal of this work is to investigate the dynamic behavior of a system undergoing impacts. More specifically, a simple impact oscillator was constructed of a horizontally shaken pendulum and rigid stop assembly covered with a “soft” polymer chosen to introduce viscoelastic effects and add model complexity.

This investigation includes comparing contact models with increasing levels of complexity to experimental observations, demonstrating interesting nonlinear behavior, and determining the ability of the contact models to accurately predict the observed nonlinear behavior using numerical simulation. This analysis removes some constraints imposed by previous works and attempts to broaden the understanding of discontinuous dynamics and expand the analysis of impact oscillators to include more refined

mathematical models when necessary. This in turn allows more complex systems to be investigated, and new types of nonlinear behavior analyzed.

Chapter 2 presents the mathematical representation of the continuous system without impact constraints and applies perturbation theory to determine an approximate analytical solution. An efficient approach to obtaining an approximate response of the discontinuous system with numerical integration is introduced and the experimental study is described.

Chapter 3 describes the contact models and identification methods used for model parameter identification of the unforced pendulum. A primary aim was to investigate parameter identification for finite time impact models. It is shown that for linear contact models, it is straightforward to determine the viscous damping parameters from the overall system response, but determining the stiffness terms requires specialized instrumentation. For nonlinear contact models, the viscous and stiffness terms are coupled, and the overall system response does not provide sufficient information for determining these parameters uniquely.

Since the discontinuous restoring force at impact provides a significant source of nonlinearity, Chapter 4 explores the rich and complex dynamics that are inherent in the discontinuous dynamical system. Period doubling bifurcations are a common and well-known route to chaos, both of which are demonstrated with numerical and experimental results. Another type of behavior which has been termed chatter is demonstrated and analyzed using the separate contact models. To the author's knowledge, this is the first published account of chatter observed in an experimental impact oscillator. Further investigations of the contact models are performed in context of the parametrically

excited system and the ability of each model to accurately predict the observed behavior is assessed.

Finally, the overall system is considered and the results are interpreted to provide information regarding the accuracy, complexity, and feasibility of several different contact models. The results are compared with that of previous works and recommendations are made for future investigations.

CHAPTER 2
PRELIMINARY FRAMEWORK

Mathematical modeling of dynamical systems has become a powerful tool in predicting and analyzing the behavior of new and existing systems. Furthermore, the power of the digital computer has introduced efficient ways of solving and analyzing complex nonlinear problems with a great deal of success. However, the majority of the analytical and computational tools that have been developed apply only to continuous dynamical systems, even though nearly all physically realizable systems will experience mechanical discontinuities such as dry friction or impact during normal operation. Investigating discontinuous dynamical systems requires understanding the limitations of continuous system methods and developing ways to apply existing knowledge to new problems.

Discontinuous dynamical systems are most commonly modeled by treating the system as a finite number of continuous subsystems related through the discontinuities [33]. This allows the use of existing methods to model the system between events and account for the discontinuities separately. The global solution is obtained by connecting the local solutions determined in each subspace. In the general case, no analytical solution exists for the local system response, and numerical integration is used to predict the system behavior. In some specific cases, such as a linear impact oscillator, an exact piecewise solution can be found providing a deeper understanding of the governing dynamics.

This chapter presents the analytical and computational tools necessary to accomplish the piecewise solution approach described above for an impacting pendulum device. The nonlinear equations of motion are developed and an approximate analytical solution is presented for the unforced pendulum. A numerical algorithm for obtaining the general nonlinear system response is explained and the experimental apparatus used to demonstrate application of these methods is described.

Pendulum Equation of Motion

Derivation of the equation of motion (EOM) for a simple pendulum shown in Figure 2.1 is straightforward using classical Newtonian mechanics or analytical dynamics.

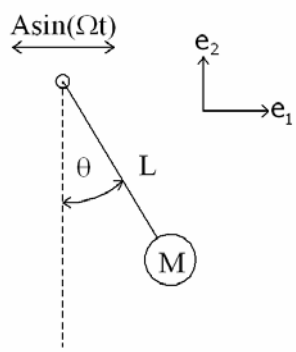

Figure 2.1: Schematic representation of a horizontally shaken pendulum

The position and velocity vectors for the center of mass of a horizontally shaken simple pendulum are given as follows, where e_1 and e_2 represent earth-fixed orthogonal unit vectors,

$$\begin{aligned} \bar{r}_{cm} &= (A\sin\Omega t + L\sin\theta)\hat{e}_1 - L\cos\theta\hat{e}_2 \\ \dot{\bar{r}}_{cm} &= (A\Omega\cos\Omega t + L\dot{\theta}\cos\theta)\hat{e}_1 + L\dot{\theta}\sin\theta\hat{e}_2 \end{aligned} \quad . \tag{1}$$

The kinetic (T) and potential (V) energy, as well as the Rayleigh dissipation function (F), are straightforward relationships,

$$T = \frac{1}{2} m \, \dot{\bar{r}}_{cm} \cdot \dot{\bar{r}}_{cm}$$

$$T = \frac{1}{2} m \, (A^2\Omega^2 \cos^2 \Omega t + 2A\Omega \cos \Omega t L \dot{\theta} \cos\theta + L^2\dot{\theta}^2 \cos^2\theta + L^2\dot{\theta}^2 \sin^2\theta) \tag{2}$$

$$T = \frac{1}{2} m \, (A^2\Omega^2 \cos^2 \Omega t + 2A\Omega \cos \Omega t L \dot{\theta} \cos\theta + L^2\dot{\theta}^2)$$

and

$$V = mgh = mgL(1 - \cos\theta) \tag{3}$$

$$F = \frac{1}{2} c \dot{\theta}^2 . \tag{4}$$

Applying Lagrange's theorem to determine the equation of motion, the following results are achieved,

$$\frac{d}{dt}\left(\frac{\partial T}{\partial \dot{\theta}}\right) - \frac{\partial T}{\partial \theta} + \frac{\partial V}{\partial \theta} + \frac{\partial F}{\partial \dot{\theta}} = 0 \tag{5}$$

$$\frac{d}{dt}\left(\frac{\partial T}{\partial \dot{\theta}}\right) = mAL\Omega(-\Omega \sin \Omega t \cos\theta - \dot{\theta} \cos \Omega t \sin\theta) + mL^2\ddot{\theta} \tag{6}$$

$$\frac{\partial T}{\partial \theta} = -mAL\Omega\dot{\theta} \cos \Omega t \sin\theta \qquad \frac{\partial V}{\partial \theta} = mgL \sin\theta \qquad \frac{\partial F}{\partial \dot{\theta}} = c\dot{\theta} . \tag{7,8,9}$$

Finally, the single degree of freedom equation of motion is given as

$$\ddot{\theta} + 2\varsigma\omega\dot{\theta} + \omega^2 \sin\theta = \frac{A}{L}\Omega^2 \sin \Omega t \cos\theta \qquad 2\zeta\omega = c/mL^2 , \quad \omega^2 = g/L . \tag{10}$$

It is convenient to non-dimensionalize the preceding equation of motion using the forcing frequency, Ω. To accomplish this, the dependent variable is rescaled using Ωt=τ, which leads to

$$\theta'' + 2\zeta\eta\theta' + \eta^2 \sin\theta = \frac{A}{L}\cos\theta\sin\tau \qquad \eta = \omega/\Omega, \tag{11}$$

where primes denote differentiation with respect to τ.

Unforced Pendulum Approximate Analytical Solution

Equation 11 is a nonlinear ordinary differential equation and an exact solution does not exist. However, for the unforced pendulum, when A=0 and η=ω, it is possible to apply perturbation theory and achieve an approximate analytical solution for the lightly damped pendulum. One such perturbation technique is the method of multiple time scales described by many authors including Meirovitch [14], Nayfeh and Balachandran [16], and Jordan [11]. Reverting back to a dimensionalized form of Equation 11 with the forcing amplitude equal to zero, the familiar planar pendulum equation of motion is

$$\ddot{\theta} + 2\zeta\omega\dot{\theta} + \omega^2 \sin\theta = 0\,. \tag{12}$$

Following the presentation by Koplow [12], a general solution is assumed in the form

$$\theta(\tau,\varepsilon) = \theta_0(\tau,\tau_1,\tau_2) + \varepsilon\theta_1(\tau,\tau_1,\tau_2) + \varepsilon^2\theta_2(\tau,\tau_1,\tau_2)\,, \tag{13}$$

where the independent time scales are defined as $\tau = t$, $\tau_1 = \varepsilon t$, and $\tau_2 = \varepsilon^2 t$. Since the independent variables have been changed, it is necessary to express the derivatives in terms of the new independent variables. Using a partial derivative expansion gives

$$\begin{aligned} \frac{d}{d\tau} &= D_0 + \varepsilon D_1 + \varepsilon^2 D_2 \\ \frac{d^2}{d\tau^2} &= D_0^2 + 2\varepsilon D_0 D_1 + 2\varepsilon^2 D_0 D_2 + \varepsilon^2 D_1^2 \end{aligned} \tag{14}$$

Rewriting the equation of motion in terms of the independent time scales, expanding the *sinθ* term in a Taylor series, and defining the parameters $\varsigma\omega = \varepsilon^2\mu$ and $-\omega^2/6 = \varepsilon^2\beta$, the approximate equation of motion becomes

$$\ddot{\theta} + 2\varepsilon^2\mu\dot{\theta} + \omega^2\theta + \varepsilon^2\beta\theta^3 = 0\,. \tag{15}$$

Substituting the assumed solution into (15) and separating into orders of epsilon yields three distinct equations.

$$\begin{aligned} &O(\varepsilon^0): D_0^2\theta_0 + \omega^2\theta_0 = 0 \\ &O(\varepsilon^1): D_0^2\theta_1 + \omega^2\theta_1 = -2D_0D_1\theta_0 \\ &O(\varepsilon^2): D_0^2\theta_2 + \omega^2\theta_2 = -2D_0D_1\theta_1 - 2D_0D_2\theta_0 - D_1^2\theta_0 - 2\mu D_0\theta_1 - \beta\theta_0^3 \end{aligned} \tag{16}$$

The general solution to (15) is found by solving each of the ordered equations in (16) in a systematic fashion. The solution to the $O(\varepsilon^0)$ equation is of the form

$$\theta_0 = A(\tau_1,\tau_2)e^{i\omega\tau} + \overline{A}(\tau_1,\tau_2)e^{-i\omega\tau}, \tag{17}$$

where the overbar denotes a complex conjugate. This solution is substituted into the $O(\varepsilon^1)$ equation obtaining

$$D_0^2\theta_1 + \omega^2\theta_1 = -2i\omega[D_1A(\tau_1,\tau_2)e^{i\omega\tau} + D_1\overline{A}(\tau_1,\tau_2)e^{-i\omega\tau}]. \tag{18}$$

The forcing term present in (18) represents a secular term which causes a resonant condition for an undamped system giving an unbounded response. Eliminating the secular terms from (18) requires that $D_1A=0$, which implies that A is a function of only the next time scale $A=A(\tau_2)$ and the solution to (18) for θ_1 is of the same form as θ_0,

$$\theta_1 = B(\tau_1,\tau_2)e^{i\omega\tau} + \overline{B}(\tau_1,\tau_2)e^{-i\omega\tau} \quad . \tag{19}$$

Substituting the expression for θ1 and θ0 into the O(ε2) equation,

$$\begin{aligned} D_0^2\theta_2 + \omega^2\theta_2 = &-2i\omega D_1B(\tau_1,\tau_2)e^{i\omega\tau} - 2i\omega D_2A(\tau_2)e^{i\omega\tau} - 2i\mu\omega A(\tau_2)e^{i\omega\tau} \\ &- \beta A(\tau_2)^3e^{3i\omega\tau} - 3\beta A(\tau_2)^2\overline{A}(\tau_2)e^{i\omega\tau} + c.c. \end{aligned} \quad , \tag{20}$$

where c.c. represents the complex conjugate of each term in (20). Eliminating secular terms from (20) results in

$$-2i\omega D_1B(\tau_1,\tau_2) - 2i\omega D_2A(\tau_2) - 2i\mu\omega A(\tau_2) - 3\beta A(\tau_2)^2\overline{A}(\tau_2) = 0. \tag{21}$$

Realizing that $D_1B = 0$ since $A=A(\tau_2)$, (21) can be subsequently reduced to

$$-2i\omega[D_2A(\tau_2)-\mu A(\tau_2)]-3\beta A(\tau_2)^2\overline{A}(\tau_2)=0. \tag{22}$$

At this point, it is convenient to express the variable A in polar form as

$$A(\tau_2)=\frac{1}{2}a(\tau_2)e^{i\phi(\tau_2)}. \tag{23}$$

Substituting (23) into (22) and separating into real and imaginary parts gives

$$\begin{aligned} a'+\mu a&=0\\ \phi'-\frac{3\beta a^2}{8\omega}&=0 \end{aligned}. \tag{24}$$

Equations (24) represent two linear first order ODE's and can be easily solved to give

$$\begin{aligned} a&=a_0e^{-\mu\tau_2}\\ \phi&=-\frac{3\beta a_0^2}{16\mu\omega}e^{-2\mu\tau_2}+\phi_0 \end{aligned}. \tag{25}$$

where a_o and ϕ_o are constants of integration. The variable a represents the amplitude of the approximate solution and ϕ represents the phase. Substituting the expressions in (25) into the assumed form of the solution in (17) and rewriting the exponential term using Euler's identity, the approximate solution for the transient motion is obtained to be

$$\theta=a_0e^{-\mu\tau_2}\cos\left(\omega\tau-\frac{3\beta a_0^2}{16\mu\omega}e^{-2\mu\tau_2}+\phi_0\right). \tag{26}$$

Reversing the substitutions made in (15) and rewriting the equation in terms of the system parameters results in

$$\theta(t)=a_0e^{-\zeta\omega t}\cos\left(\omega t-\frac{a_0^2}{32\varsigma}e^{-2\zeta\omega t}+\phi_0\right). \tag{27}$$

The derivative of (27) is found by differentiating (17) with respect to the time scale τ, realizing that A=A(τ_2) and is treated as a constant during differentiation which gives

$$\theta_0' = i\omega\, A(\tau_2)e^{i\omega\tau} - i\omega\, \overline{A}(\tau_2)e^{-i\omega\tilde{\tau}} \tag{28}$$

Substituting the expressions for a and φ given in (25) into (28) gives

$$\dot{\theta}(t) = -a_o \omega e^{-\varsigma\omega t} \sin\left(\omega t + \frac{a_o^2}{32\varsigma} e^{-2\varsigma\omega t} + \phi_o \right). \tag{29}$$

This expression is notably different than the result obtained by differentiating (27) directly but remains an appropriate first order approximation.

In general, the parameters a_o and ϕ_o must be related to the initial conditions $\theta(0)$ and $\dot{\theta}(0)$ resulting in two equations and two unknowns which must be solved simultaneously using a numerical root finding algorithm. However, in the case that either of the initial conditions are zero, a simple relationship results and the parameters a_o and ϕ_o can be specified uniquely as a function of $\theta(0)$ and $\dot{\theta}(0)$. The results are easily obtained from the equations above and presented below for convenience.

Case I: $\theta(0) = \theta_0$ and $\dot{\theta}(0) = 0$

$$\theta(t) = \theta_0 e^{-\varsigma\omega t} \cos\left[\omega t + \frac{\theta_0^2}{32\varsigma}(e^{-2\varsigma\omega t} - 1) \right] \tag{30}$$

$$\dot{\theta}(t) = -\theta_0 \omega e^{-\varsigma\omega t} \sin\left[\omega t + \frac{\theta_0^2}{32\varsigma}(e^{-2\varsigma\omega t} - 1) \right] \tag{31}$$

Case II: $\theta(0) = 0$ and $\dot{\theta}(0) = v_0$

$$\theta(t) = -\frac{v_0}{\omega} e^{-\varsigma\omega t} \sin\left[\omega t + \frac{v_0^2}{32\varsigma\omega^2}(e^{-2\varsigma\omega t} - 1) \right] \tag{32}$$

$$\dot{\theta}(t) = -v_0 e^{-\varsigma\omega t} \cos\left[\omega t + \frac{v_0^2}{32\varsigma\omega^2}(e^{-2\varsigma\omega t} - 1) \right] \tag{33}$$

Equations (30)-(33) represent approximate analytical solutions to the unforced pendulum continuous equation of motion for known initial conditions. These results will

be useful in identifying the system parameters ω and ς for the oscillating pendulum, obtaining a piecewise continuous approximate solution for the impacting pendulum, and estimating impact parameters from experimental observations.

Numerical Simulation

When discontinuous functions are used to model discontinuous systems, the response can be readily obtained using conventional numerical algorithms. The algorithms must be modified slightly to include detection of the discontinuity and calculation of the precise time when the discontinuity occurs [33]. However, special attention must be given to numerical error. Slight changes in the states of the system when the discontinuity occurs may give largely different global predictions. This is a phenomenon associated with nonlinear dynamic systems where, unlike linear systems, small changes in nonlinear systems may have large effects on the global behavior.

This approach considers an initially continuous nonautonomous system of the form

$$\frac{dx}{dt} = f(t; x, p)\,, \tag{34}$$

where $x = [x_1, x_2, \ldots, x_n]^T$ is the state space vector and $p = [p_1, p_2, \ldots, p_n]^T$ is a vector of system parameters. In order to account for the k discontinuities, an appropriate switch function, Φ_k, governed by the flow of the system is required. A discontinuity for the kth subspace is detected when

$$\Phi_k(t; x) = 0\,. \tag{35}$$

When the discontinuity is detected, the system is governed by a new equation of motion and a mapping G is applied,

$$G : f_i(t; x, p), \qquad x_-^{(k)} \rightarrow x_+^{(k)} \tag{36}$$

This process is continued until the next discontinuity is encountered or the desired exit conditions are reached.

Applying the mapping function G to the system precisely at $\Phi_k(t;x)=0$ implies that the system states are known exactly at the instant the discontinuity occurs. However, this is rarely the case. In fact, a discontinuity is detected at the jth time step by evaluating the condition $\Phi^j\Phi^{j-1}<0$. Once detected, the states of the system at the time the discontinuity occurred, ξ^*, must be estimated using an approximation method such as interpolation or bisection [33]. This approximation introduces error into the computation. Depending on the system, this error may or may not affect the accuracy of the global prediction.

As an alternative to the approximation method above, Henon suggested a method for predicting the system response to a motion limiting discontinuity using a simple variable transformation [9]. Henon's method is based on classical numerical integration schemes, such as one of the many Runge Kutta algorithms, which represents the differential state space as a set of n algebraic equations. During integration, when a discontinuity is detected by $\Phi^j\Phi^{j-1}<0$ at the jth time step, the algorithm steps back to the last time step before the discontinuity and computes the precise time necessary to achieve $\Phi_k(t;x)=0$. In this manner, the need for an approximation of the states at the discontinuity is eliminated and the overall accuracy of the model is enhanced. Henon's method may be used when slight errors in the computation of the system response result in dramatic effects on the global behavior.

The methods described so far apply to any discontinuous system that can be represented in state space form. No limitations have been placed on the mapping

function G, the switch function Φ, or the number of discontinuities *k*. Applying this approach to the impacting pendulum used in this investigation is straightforward. Referring to the planar pendulum equation of motion in non-dimensional form

$$\theta'' + 2\zeta\eta\theta' + \eta^2 \sin\theta = \frac{A}{L}\cos\theta \sin\tau \qquad \eta = \omega/\Omega, \tag{37}$$

the equation can be written in state space form as

$$\begin{aligned} x_1' &= x_2 \\ x_2' &= -2\zeta\eta\, x_2 - \eta^2 \sin x_1 + \frac{A}{L}\cos x_1 \sin\tau \end{aligned} \tag{38}$$

where the substitutions $x_1 = \theta$ [rad] and $x_2 = \theta'$ [rad/sec] have been made. Since the impacting pendulum experiences a discontinuity at $x_1 = 0$ [rad], the natural choice for the switch function is $\Phi_k(t;x) = x_1$. The choice for the mapping function G and the number of discontinuities used to model the impacting pendulum is the subject of the remainder of this investigation. In general, the mapping function G may be an algebraic or differential relationship representing an instantaneous or finite time contact model. Since the experimental device only has a single rigid stop, the number of discontinuities will be *k = 1*.

The above procedures were implemented for the impacting pendulum using a variable step fourth-order Runge Kutta ODE solver. The discontinuities were detected using the switch function $\Phi_k(t;x) = 0$ and linear interpolation was performed to estimate the time at which the zero crossing occurred. Henon's method was not considered necessary since the contact duration and maximum approach were very small compared to the overall system response.

Experimental Apparatus

The impacting pendulum device of interest consists of a 1/8" thick threaded steel shaft connected to a 1 inch (25.4mm) diameter, type 303 stainless steel knob with a mass of m = 20 g. The impacting material consists of a 1/8" thick, 70A Durometer polyurethane material with a 0.005 inch thick acrylic adhesive on the non-impact surface. The polyurethane material was chosen for its viscoelastic material properties. The separation angle of the pendulum rod from the vertical is captured through the use of a potentiometer and the amplitude of the harmonic displacement is captured with an optical laser. The pendulum's pivot point is subjected to a horizontal sinusoidal forcing through the use of a shaker. Figure 2.2 depicts a dimensioned schematic of the experimental device.

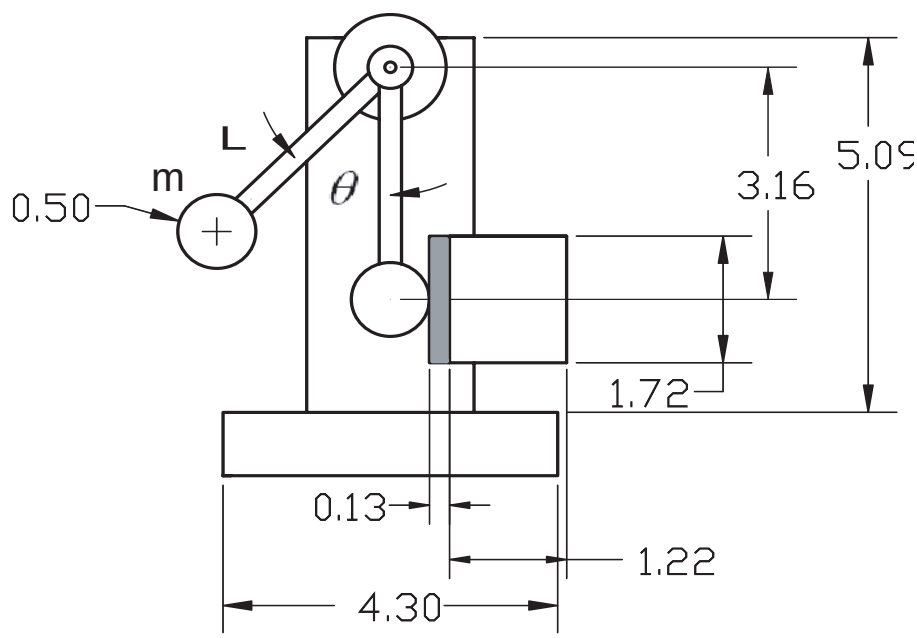

Figure 2.2: Schematic of experimental pendulum device (all dimensions in inches)

The recorded time series were filtered to reduce noise using an anti-aliasing filter with a sampling frequency of 1 kHz and a cutoff frequency of 50Hz. The pendulum natural frequency is on the order of 2Hz so a cutoff frequency of around 10Hz would have given sufficiently accurate results with the lowest amount of noise, but it was determined that the impacts were not entirely captured at this frequency. The cutoff frequency of 50Hz allowed more noise to pass, but reduced most of the 60Hz electrical noise and sufficiently captured the impact events.

Data were collected for three different scenarios. Freefall data were collected for a series of experiments with the rigid stop removed. These data were used for determining the pendulum freefall parameters ς and ω. Transient data were collected for the unforced impacting pendulum for use in characterizing the impact parameters and validating impact models for the simplest possible case. Periodic impacting data were collected at a range of driving frequencies (1- 15 Hz) and forcing amplitudes (1-5mm), subject to the shaker limitations. Discrete frequency sweeps were performed at constant amplitude (3 mm) and constant voltage.

The single degree of freedom equation of motion previously derived for the system includes multiple unknown system parameters including the natural frequency, ω_n, the damping, ς. In order to simulate the dynamics, these parameters must be obtained from the experimental response of the system.

Determination of the damping and natural frequency is straight forward and can be performed in a number of ways. In the present analysis, the impact surface was removed which allowed the pendulum to oscillate at arbitrarily large angles. Perturbations were applied to the pendulum and the response was measured. A nonlinear least-squares

optimization routine, suggested by Koplow [12], was then used to determine the parameter values that "best" fit the experimental data using the second order multiple scales solution. Figure 2.3 shows a snapshot of the results from this analysis. The natural frequency was determined to be 13.47 +/- 0.05 rad/sec (2.144 +/ 0.008 Hz) and the damping was found to be 0.0017 +/- .0001.

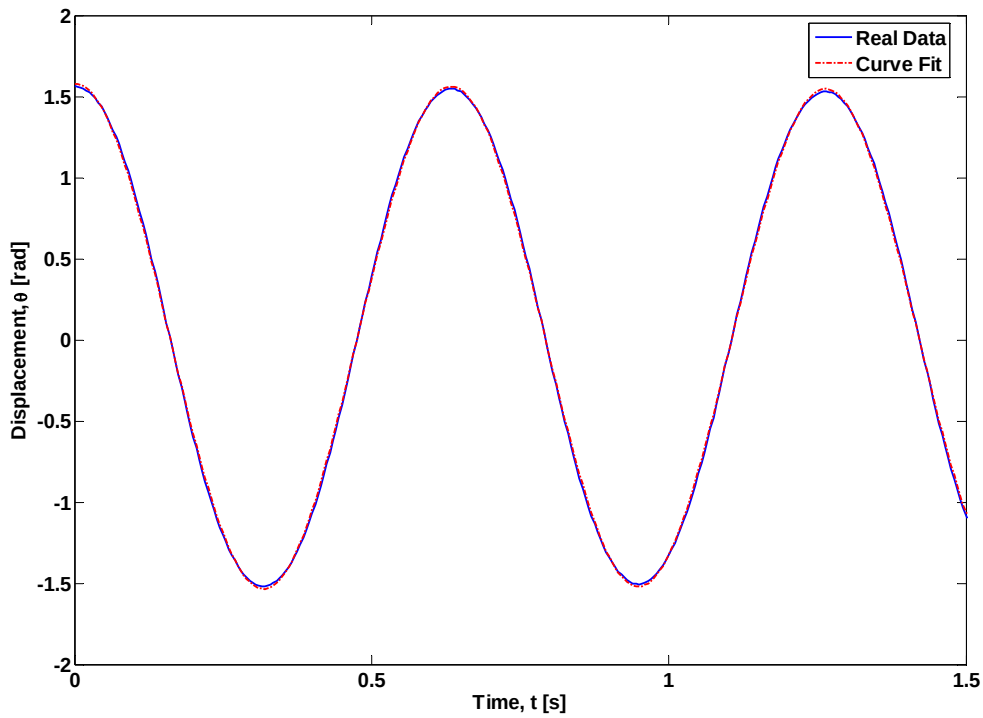

Figure 2.3: Free oscillation curve fitting

Using the approach above, the effective length of the pendulum was determined to be 2.8 +/- .02 in (71 +/- 0.5 mm). The effective length is the "mathematical" length of the pendulum with a massless rod, determined from the natural frequency as $L = g/\omega^2$. In each case, the uncertainty was estimated by assuming a normal error distribution and computing the error as $\hat{\varepsilon} = 2\hat{\sigma}$ where $\hat{\sigma}$ is the sample standard deviation.

CHAPTER 3
CONTACT MODELING AND PARAMETER IDENTIFICATION

The study of contact modeling is nearly as old as the study of dynamics itself. In fact, Isaac Newton devoted a great deal of effort to characterize impacts as an illustration of his third law, that every action has an equal and opposite reaction [17]. The most commonly used impact model, the kinematic coefficient of restitution, is credited to Isaac Newton and his studies on two impacting spheres. Newton was the first to realize that not all impacts are elastic, and that the degree of inelasticity is in fact a property of the colliding materials [27]. Despite the early advances in contact modeling, the subject is still under thorough investigation today. Contact modeling has been extended from the simple coefficient of restitution model to full three-dimensional models accounting for slip, friction, and vibration [27].

Due to the underlying complexities inherent in describing dynamics of rigid bodies in contact, a vast number of mathematical models have been investigated. W.J. Stronge [27] presents a large collection of models including the kinematic and energetic coefficients of restitution as a linear function of the normal impulse, and the Maxwell and Kelvin-Voight models for linear compliance. Stronge and Chatterjee [5] make use of a class of nonlinear compliance models proposed by Walton [32]. Simon [25] suggested a hybrid model for spherical indenters based on earlier work by Hertz. Hunt and Crossley [10] expounded on the damping associated with the Kelvin-Voight model and the family of models proposed by Hertz by expressing the damping as an equivalent coefficient of restitution. More recently, Půst and Peterka [20] have investigated the use of Hertz's

model to analyze "soft" impacts with promising results and M. Van Zeebroeck et al. [30] have used variants of Hertz's work in studying damage to biological materials. All of these models have common characteristics and present a wide range of application.

In the present work, three models representing different levels of complexity have been chosen for application to the experimental system. These include the coefficient of restitution, lumped parameter, and the Hertzian models. The coefficient of restitution is by far the most commonly used model for single degree of freedom systems. The lumped parameter and Hertz representations are compliance models. Whereas the coefficient of restitution model assumes an instantaneous impact, compliance models attempt to capture the relative displacement and contact force during impact.

The coefficient of restitution, lumped parameter, and Hertzian models have many variants. The characteristics of an impact are heavily dependent on many things including the material properties of each body, the relative impact velocity, the impact configuration, the geometrical form, the degree of deformation, and even the temperature of each body involved in the collision [3]. Describing each of these relationships directly is nearly impossible due to lack of fundamental theory or insufficient test data. This has given rise to many different models to fit many different scenarios. Unfortunately, it is impossible to expect any one model to perfectly describe the impact relationship under all conditions, so different models will demonstrate success in different applications [3]. One of the objectives of this paper is to investigate how these models interact and apply to the test case of interest.

The three aforementioned models were chosen because they represent a wide range of applicability with increasing degrees of complexity. The coefficient of restitution

model is by far the simplest, based completely on an algebraic relationship. The lumped parameter is slightly more complicated and is based on a lumped elements common to vibration and linear system theory (i.e., the spring and dashpot). The Hertzian model is the most complicated because it attempts to take into account the geometric form of the indenter, introducing a geometric nonlinearity. One hopes that by increasing the fidelity and complexity of the mathematical model, a higher level of accuracy will be achieved.

The relative "difficulty" of each model is related to the type of the model, either algebraic or differential, and the form of each model, either linear or nonlinear. As previously described, the discontinuous nature of the problem typically precludes any analytical solution and requires the use of a digital computer for analysis. This being the case, the difficulty of each model may seem trivial, since modern day computers are quite capable of solving problems for which analytical solutions do not exist. However, the difficulty arises in implementing each of the above models for a realistic system. Each of the models includes one or more unknown parameters which must be determined from experimental observations. For linear models, this is straightforward when enough information is available. For nonlinear models, the parameters are often coupled and it may be difficult if not impossible to estimate the parameters uniquely. In either case, attention must be given to the type and level of resolution of the data collected. It will be shown that energy dissipation parameters such as damping may be estimated when only the global system behavior is known, whereas estimating stiffness parameters usually requires information acquired during impact, such as the duration or maximum approach.

The purpose of this chapter is to give a brief introduction for each of the selected models, discuss relationships between the models, and provide methods for estimating

the model parameters from experimental data when possible. In accomplishing this, it is desirable to begin with the unforced pendulum experiment to avoid undue complication. These results are referred to as *transient*, as opposed to the *steady state* results presented for the forced pendulum experiment.

Coefficient of Restitution

In every physical experiment involving impact, non-frictional energy dissipation occurs due to inelastic deformation, elastic vibrations, and/or viscoelasticity. When the impact is of sufficiently short duration compared to the overall system behavior, this loss in kinetic energy may be quantified as a coefficient of restitution.

General Theory

For collinear impact, Stronge [27] shows that the relative velocity during impact is a linear function of the normal impulse,

$$v = v_0 + m^{-1} p \,, \tag{1}$$

where the initial velocity of impact is $v_0 < 0$. Here, m is the effective mass defined as

$$m = (M^{-1} + M'^{-1})^{-1} \tag{2}$$

where M is the mass of body B, and M′ is the mass of body B′. In the special case that one of the bodies is a rigid stop, as in the impact pendulum under consideration, M′ = ∞ and equation (2) reduces to $m = M$, the effective mass of the pendulum. The impulse can be described in terms of the contact force as

$$p = \int_0^t F(t)dt \,. \tag{3}$$

The reaction impulse which brings the bodies to zero relative velocity is termed the *normal impulse for compression*, and from equation (1) is given by

$$p_c = -mv_0 \,. \tag{4}$$

A related quantity is the value of the *impulse at separation*, given by evaluating the integral (3) from over the contact duration, t_c. During compression, the kinetic energy is transformed into strain energy through work done by the contact force. During restitution, the elastic portion of the strain energy is transformed back into kinetic energy by the contact force. Stronge gives these relationships for a direct impact as

$$W(p_c) = \int_0^{p_c} v(p)dp = v_0 p_c + \frac{1}{2} m^{-1} p_c^2 = -\frac{1}{2} m^{-1} v_0^2 \tag{5}$$

$$W(p_f) - W(p_c) = \int_{p_c}^{p_f} (v_0 + m^{-1} p)dp = \frac{m v_0^2}{2}\left(1 - \frac{p_f}{p_c}\right)^2 . \tag{6}$$

It follows that the total energy dissipated during the collision is related to the work done during compression and the energy released during restitution. In fact, the square of the coefficient of restitution, r^2, is the negative of the ratio of the elastic strain energy released during restitution to the internal energy of deformation absorbed during compression,

$$r^2 = -\frac{W(p_f) - W(p_c)}{W(p_c)} \tag{7}$$

Equation (7) is referred to as the *energetic coefficient of restitution* and is valid for all impact configurations. In the special case of a collinear impact, the expressions from (5) and (6) can be used to reduce (7) to the *kinematic coefficient of restitution*

$$r = \frac{-v_f}{v_0}, \tag{8}$$

and the *kinetic coefficient of restitution*

$$r = -\frac{p_f - p_c}{p_f} . \tag{9}$$

The kinematic coefficient of restitution was first introduced by Newton (1687). The kinetic coefficient of restitution was first introduced by Poisson (1811), who recognized that it is equivalent to the kinematic coefficient of restitution if the direction of slip is constant. The energetic, kinematic, and kinetic coefficients of restitution are equivalent unless (1) the bodies are rough, (2) the configuration is eccentric, and (3) the direction of slip varies during the collision [27]. In this thesis, these assumptions are satisfactory and the kinematic coefficient of restitution will be used.

Contact Parameter Identification

The coefficient of restitution is typically an experimentally determined value. It is widely known that the value of the coefficient is not constant for every impact, but dependent upon the impact velocity, material properties, the shape of the impacting bodies, and degree of deformation [7]. The basic relationship for the coefficient of restitution observed experimentally is that the value is highest at low impact velocities and may be very near unity. With an increase in impact velocity, first the coefficient of restitution decreases rapidly, and then maintains a nearly constant value [3]. This relationship is predicted by viscous theory which supposes energy dissipation proportional to the velocity.

Application of the coefficient of restitution model to the impacting pendulum is straightforward and is given by,

$$\begin{aligned} &\theta'' + 2\zeta\eta\theta' + \eta^2 \sin\theta = \frac{A}{L}\cos\theta\sin\tau && \theta > 0 \\ &\theta'_+ = r\,\theta'_- && \theta = 0 \end{aligned} \quad . \tag{10}$$

In addition to the simplicity the coefficient of restitution, an added benefit of using this widespread model is the ability to readily determine its value from an experimental

system. Determination of the coefficient of restitution, r, from the system response characteristics was accomplished using the 2nd order multiple scales solution. In order to determine the coefficient of restitution experimentally, an estimate of the velocity at incidence and the velocity at separation must be determined. Due to measurement noise near the impact point, it would be impossible to determine these values directly from the displacement time series or reconstructed state vector. Alternatively, a method was devised in which consecutive peaks obtained from the experimental time series were related to the separation and impact velocities. The results obtained from the multiples scales solution are repeated here for convenience.

Case I: $\theta(0) = \theta_0$ and $\dot{\theta}(0) = 0$

$$\theta(t) = \theta_0 e^{-\varsigma\omega t} \cos\left[\omega t + \frac{\theta_0^2}{32\varsigma}(e^{-2\varsigma\omega t} - 1)\right] \tag{11}$$

$$\dot{\theta}(t) = -\theta_0 \omega e^{-\varsigma\omega t} \sin\left[\omega t + \frac{\theta_0^2}{32\varsigma}(e^{-2\varsigma\omega t} - 1)\right] \tag{12}$$

Case II: $\theta(0) = 0$ and $\dot{\theta}(0) = v_0$

$$\theta(t) = -\frac{v_0}{\omega} e^{-\varsigma\omega t} \sin\left[\omega t + \frac{v_0^2}{32\varsigma\omega^2}(e^{-2\varsigma\omega t} - 1)\right] \tag{13}$$

$$\dot{\theta}(t) = -v_0 e^{-\varsigma\omega t} \cos\left[\omega t + \frac{v_0^2}{32\varsigma\omega^2}(e^{-2\varsigma\omega t} - 1)\right] \tag{14}$$

The analytical solution presented in case I can be used to solve for the time and velocity at which the pendulum crosses zero based on a specified initial angle. The solution presented in case II may be used to iteratively solve for the initial velocity that causes a specific peak value at a given time. Together, the solutions can be used to determine the velocity prior to impact and the velocity at separation when any two

successive peaks are provided. Figure 3.1 depicts a simulated transient response in which the coefficient of restitution was chosen to be 0.60. The method outlined above was then used to determine the coefficient of restitution from the successive peaks to within .002% error.

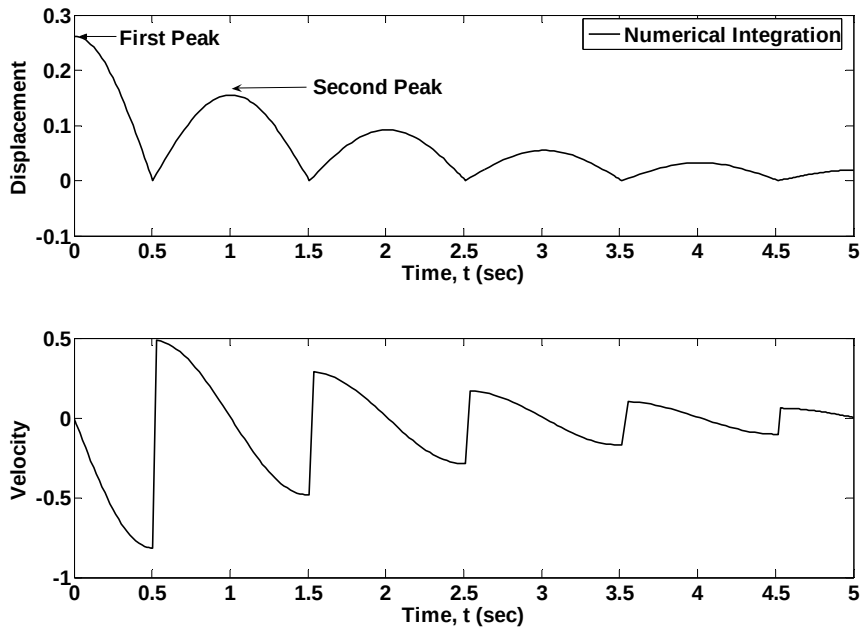

Figure 3.1: Determination of coefficient of restitution from successive peaks

This procedure was used repeatedly to determine the coefficient of restitution from transient experimental time series. The experimental coefficient of restitution was found to be 0.577 +/- 0.098. It should be noted that the uncertainty in this case is 17% of the average value. As expected, the coefficient of restitution was found to be a function of impact velocity, ranging in from .479 to .675 depending on the magnitude of v_0. This limitation is a result of the viscoelastic properties of the material.

Modeling the Transient System Response

While no general solution to the discontinuous equation of motion for the impacting pendulum exists, it is possible to determine a piecewise analytical solution.

The piecewise analytical solution is based on the assumption that the impacting pendulum behaves essentially the same as the free pendulum over short intervals between contacts. Thus the multiple scales solution previously derived can be used to determine the system response treating each impact as a "starting point" with distinct initial conditions, similar to the approach used for numerical simulation. This approach provided good match with the simulated response for relatively large initial displacements. Figure 3.2 depicts a comparison of the numerical simulation and analytical solution for an initial displacement angle of 45˚.

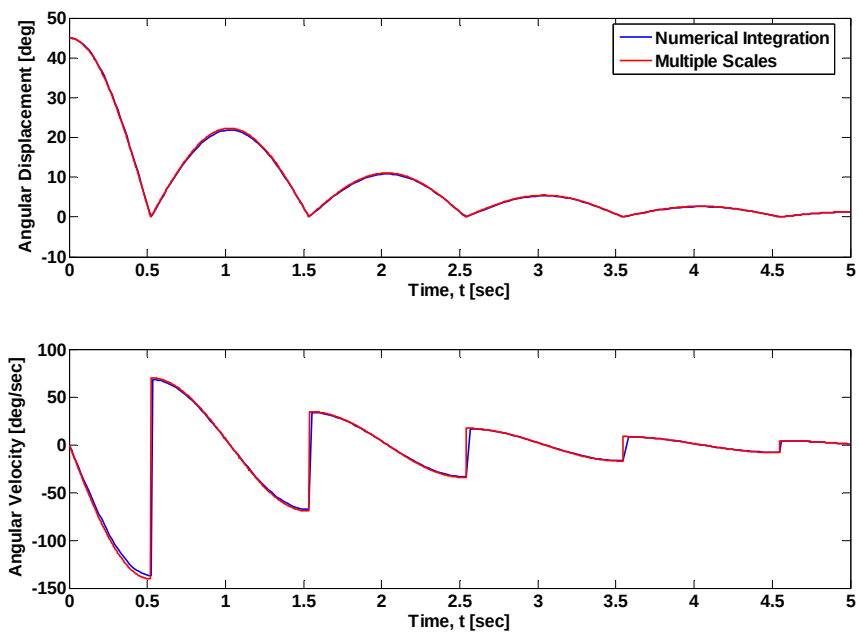

Figure 3.2: Comparison of multiple scales solution and numerical integration

The first step in comparing the numerical and experimental results for the impacting pendulum is to consider the transient motion of the pendulum with no base excitation. The results are similar to the results used to determine the coefficient of restitution from experimental data. Figure 3.3 shows an example of the transient case

comparing experimental, analytical, and numerical solutions for an initial angle of approximately 45˚. It is clear that the results are in excellent agreement.

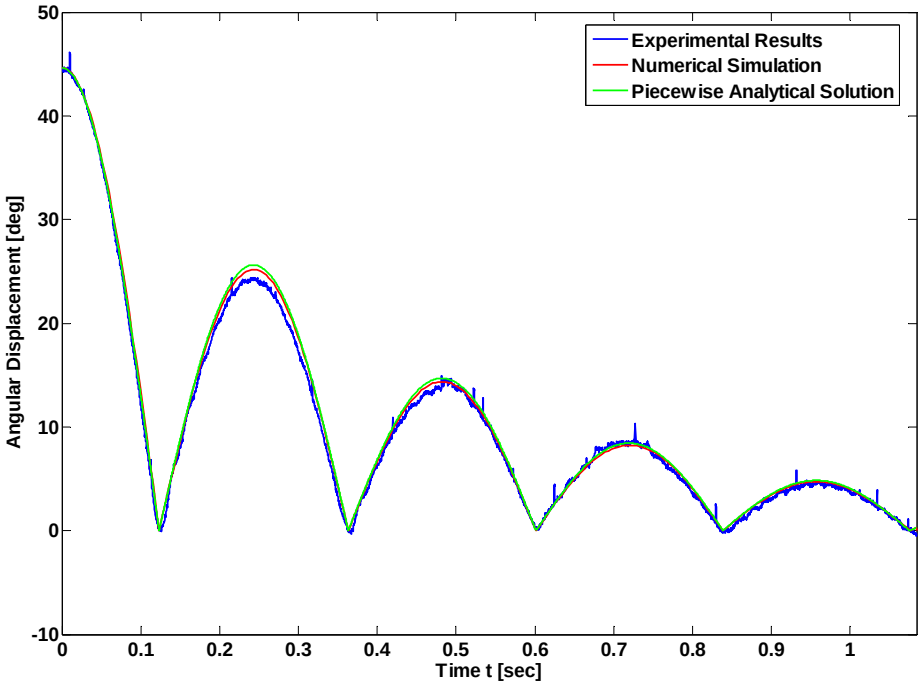

Figure 3.3: Comparison of experimental results with piecewise analytical solution and numerical integration for r = 0.577.

From close investigation of Figure 3.3, it is apparent that the numerical and analytical solutions over-predict the peak amplitude for the first two peaks and show excellent agreement with the final two peaks. Furthermore, if the time series were carried out further, the analytical and numerical solutions would under-predict the peak values. This is a manifestation of the averaged coefficient of restitution and the dependency of the coefficient of restitution on the impact velocity. The averaged value works well for average size peaks, but over-predicts large peaks and under-predicts small peaks.

Lumped Parameter Model

In many cases, an instantaneous contact model is insufficient to model the impact dynamics and a compliance model must be used. The compliance model has the added benefit of predicting the motion during impact at the cost of a more complex model.

A Linear Compliance Model

The simplest compliance models are the Maxwell and Kelvin-Voight models consisting of a linear spring and dashpot [10, 27]. The Kelvin-Voight model uses a linear spring and dashpot in parallel, whereas the Maxwell model uses the spring and dashpot in series. Both models result in an equation of motion during impact of

$$\ddot{x} + 2\gamma\omega_0\dot{x} + \omega_0^2 x = 0\,, \tag{15}$$

based on a contact force of

$$F = -c\dot{x} - kx\,. \tag{16}$$

In Kelvin-Voight model, x is identical to the linear displacement $x = L\sin\theta$, and in the Maxwell model, x is the *relative* linear displacement between the spring and dashpot. In (15), the damping during contact has been labeled γ to differentiate from the damping during free flight, ς. Likewise, the natural frequency during impact, ω_0, is different from the pendulum natural frequency, ω_n. For the Kelvin-Voight approximation, the piecewise model can be expressed as

$$\begin{aligned} &\ddot{\theta} + 2\varsigma\omega_n\dot{\theta} + \omega_n^2\theta = 0 \qquad \theta > 0 \\ &\ddot{x} + 2\gamma\omega_0\dot{x} + \omega_0^2 x = 0 \qquad \theta \le 0 \\ &x = L\sin\theta \end{aligned} \tag{17}$$

Equation (15) is a well known form and it is straightforward to determine the response during contact when the impact velocity is known. Solving for the final

velocity, an equivalent coefficient of restitution can be derived that characterizes the loss of kinetic energy but remains independent of the impact speed.

The solution to (15) for the period of contact is a half of a damped sine wave given by

$$x(t) = -\omega_d^{-1} v_0 e^{-\gamma\omega_0 t} \sin(\omega_d t), \qquad 0 \le t \le \pi/\omega_d \ , \tag{18}$$

subject to the initial conditions

$$x(0) = 0, \quad \dot{x}(0) = -v_0 \ . \tag{19}$$

In (18), ω_d is the damped natural frequency given by $\omega_d = \omega_0\sqrt{1-\gamma^2}$. The velocity at separation, v_f, is determined by differentiating (18) and evaluating at $t_c = \pi/\omega_d$,

$$v_f = v_0 e^{-\gamma\pi/\sqrt{1-\gamma^2}} \ , \tag{20}$$

which gives the equivalent coefficient of restitution directly as

$$r = \frac{v_f}{v_0} = e^{-\gamma\pi/\sqrt{1-\gamma^2}} \ . \tag{21}$$

From equation (21), it is clear that the coefficient of restitution is a function only of the damping, γ, and not the impact velocity v_0. Thus, the Kelvin-Voight model (and equivalently the Maxwell model) provides a compliance prediction where the damping is specified to achieve a desired coefficient of restitution. Using the coefficient determined in the previous section, r = 0.577, the damping parameter is determined to be $\gamma = 0.18$.

Implementing (15) requires the determination of the natural frequency during impact, ω_0, from the observed experimental response. However, the lumped parameter model predicts a contact duration, $t_c = \pi/\omega_d$, that is independent of the initial or final velocities. Therefore, whereas the damping was estimated from the overall system behavior (relative peaks), which is easily measurable, estimating the natural frequency of

impact requires either the impact duration or the maximum approach. It is much more difficult to measure these quantities with sufficient precision.

Although many novel ways of obtaining the contact duration or maximum approach may be employed, time and financial constraints precluded the use of specialized instrumentation to achieve this. An alternative, less-rigorous, method has been used to estimate the time in contact by using the observed shift in natural frequency between the freely oscillating pendulum and the impacting pendulum. The natural frequency of the pendulum was previously determined to be $\omega_n = 13.47$ rad/sec. Observed experimental impacts indicated that the natural frequency of the impacting pendulum was approximately $\omega_0 = 13.25$ rad/sec. This "shift" in natural frequency is assumed to be due entirely to the time in contact. Using the relationship $T = 1/f_n = 2\pi/\omega_n$, where T is the period of oscillation, the time in contact,

$$t_c = \frac{T_2 - T_1}{2} = \pi(\omega_2^{-1} - \omega_1^{-1}), \tag{22}$$

was computed to be $t_c = 0.0044$ sec. This gives a damped natural frequency of $\omega_d = 715.6$ rad/sec and a natural frequency of impact of $\omega_0 = 727.5$ rad/sec for $\gamma = 0.18$. Figure 3.4 shows a comparison of the transient results obtained using the Kelvin-Voight model with experimental measurements. The results are in good agreement with a slight underprediction of the peak response for lower impact velocities.

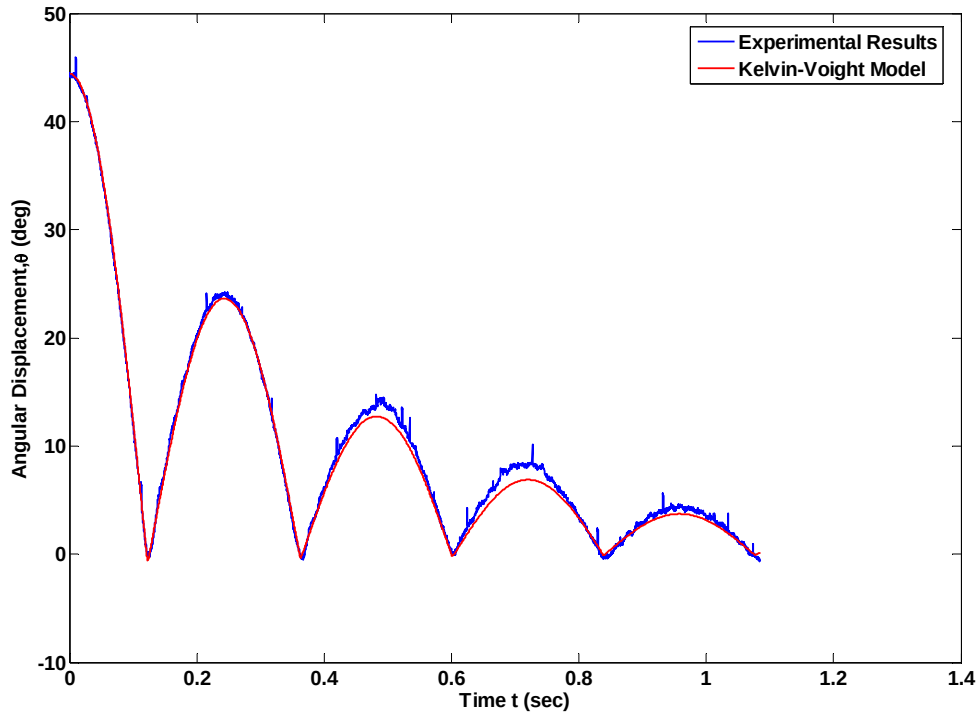

Figure 3.4: Comparison of experimental results with Kelvin-Voight model for $\gamma = 0.18$ and $\omega_0 = 727.5$ rad/sec.

A Nonlinear Compliance Model

Both of the models discussed this far, the kinematic coefficient of restitution and the Kelvin-Voight models, use an equivalent coefficient of restitution that remains constant. It follows that the same trend may be observed for both models. Namely, that the average coefficient of restitution overpredicts the peak response for large impact velocities and underpredicts the peak response for small impact velocities. This trend is in agreement with viscoelastic theory and the experimental results observed by Goldsmith [7].

A slightly more complex nonlinear discrete compliance model suggested by Walton [32] and employed by Stronge [27] and Chatterjee [5], provides an equivalent

coefficient of restitution that decreases with increasing relative impact velocity. The contact force is given by

$$F = -c\,|\,x\,|\,\dot{x} - kx\,, \tag{23}$$

with an equation of motion of the form,

$$m\ddot{x} - c\,x\,\dot{x} + kx = 0 \qquad \dot{x}(0) = v_0 < 0\,. \tag{24}$$

In (24), the negative value of the impact velocity, v_0, has been taken into account to remove the absolute value sign. Following the presentation by Stronge, (24) can be written as

$$Z\frac{dZ}{dX} + X(1-Z) = 0 \tag{25}$$

by making the substitutions

$$X = \frac{cx}{\sqrt{mk}} = \frac{c\,\omega_0 x}{k}, \qquad Z = \frac{c\dot{x}}{k}, \tag{26}$$

where

$$\frac{dZ}{dX} = \frac{dZ}{dt}\frac{dt}{dX} = \frac{1}{\omega_0}\frac{d\dot{x}}{dx} \qquad \text{and} \qquad \ddot{x} = \dot{x}\frac{d\dot{x}}{dx}\,. \tag{27}$$

The expression (25) is integrated to obtain

$$Z - Z_0 + \ln\left(\frac{1-Z}{1-Z_0}\right) = \frac{X^2}{2}\,. \tag{28}$$

By evaluating (28) at separation, $X=0$, and $Z = Z_f$, the equivalent coefficient of restitution, $r = Z_f/Z_0$, can be found using a nonlinear root finding algorithm. Chatterjee has identified a close approximation for this curve as

$$r \approx (-Z_0 + e^{0.4Z_0})^{-1}\,. \tag{29}$$

This relationship is depicted in Figure 3.5.

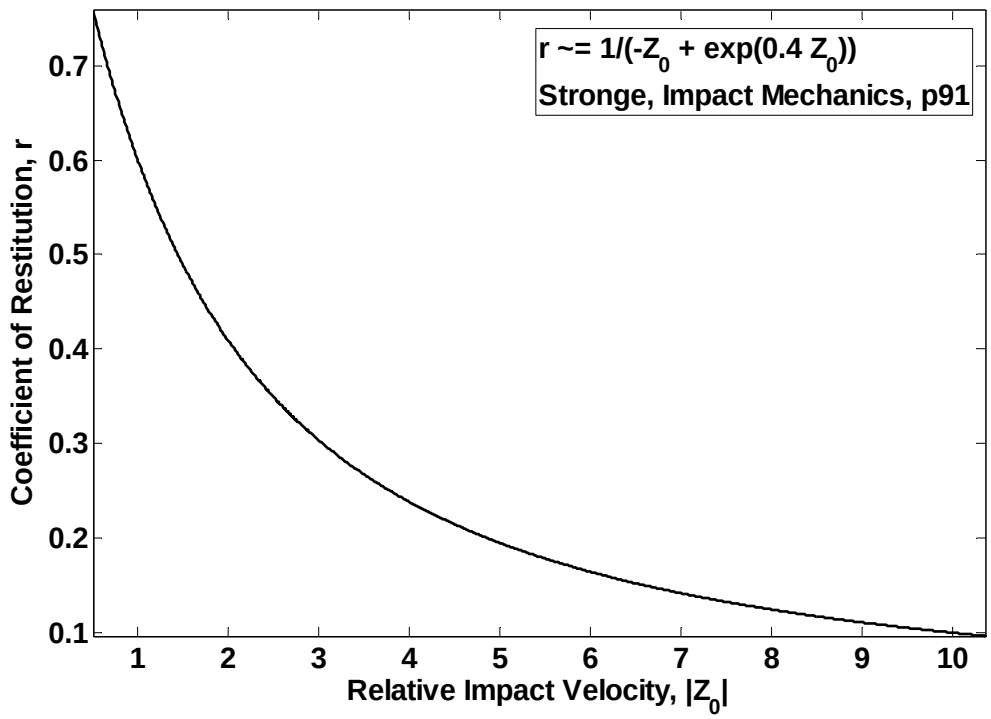

Figure 3.5: Effect of viscoelasticity on the equivalent coefficient of restitution as suggested by Chatterjee and Stronge.

To implement this model, it is necessary to determine the parameters c and k from the experimental time series. The impact velocity, v_0, separation velocity, v_f, and the equivalent coefficient of restitution were determined using the relative peaks as previously described. The ratio of c/k as it appears in $Z_0 = cv_0/k$ was determined by using a nonlinear root finder to solve

$$\lambda(v_f - v_0) + \ln\left(\frac{1-\lambda v_f}{1-\lambda v_0}\right) = 0\,, \tag{30}$$

where $\lambda = c/k$.

Unfortunately, this approach was very sensitive to uncertainty in the incidence and separation velocity estimates, which gave a wide range of possible λ values. Furthermore, through a manual search for suitable values, it was determined that the contact model was not capable of matching experimentally observed trends for the

current system. Figure 3.6 shows results obtained for λ = 0.1 and c = 1000 Ns/m (k = 1.0e4 N/m).

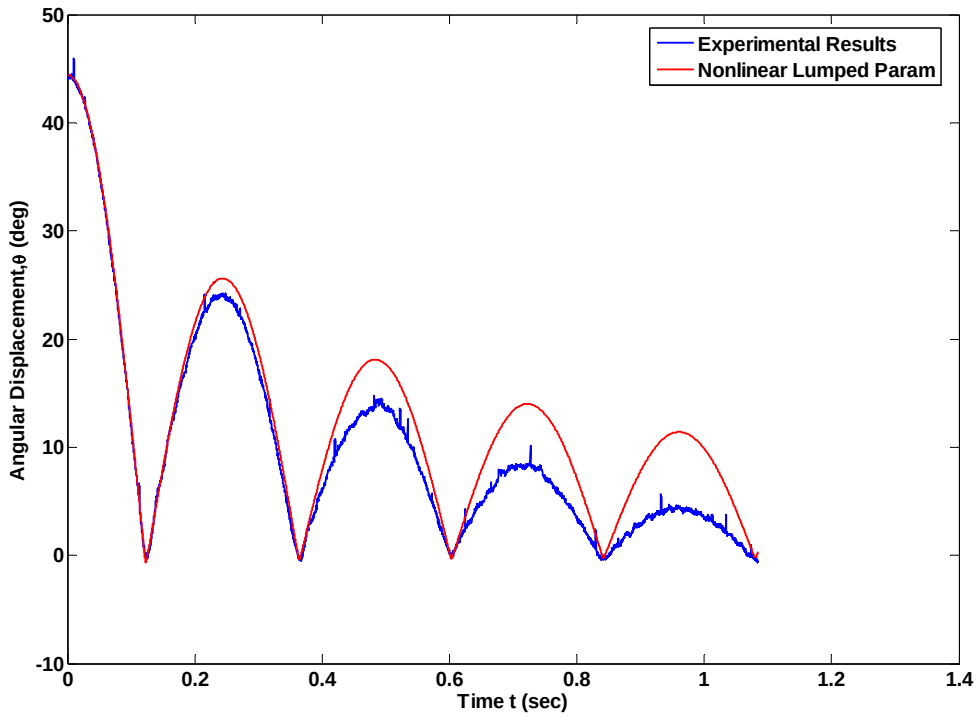

Figure 3.6: Comparison of experimental results with nonlinear lumped parameter model for λ = 0.1 and c = 1000 Ns/m (k = 1.0e4 N/m).

Referring back to Figures 3.3 and 3.4, predictions using the coefficient of restitution and Kelvin-Voight model, it is clear that the equivalent coefficient of restitution is changing relatively slowly with increasing impact velocity. The nonlinear lumped parameter model fails to match experimental results because the rate of decrease of the coefficient of restitution predicted by (29) and depicted in Figure 3.5 is too aggressive for the material under consideration. This relationship may be better suited for materials with a higher degree of viscoelasticity.

Hertzian Contact Model

The viscoelastic compliance models previously described have the added advantage of describing the energy dissipation as a function of impact velocity but remain a simplified idealization of the actual system. This section presents a simplistic *continuum* model, which represents the next step in model complexity.

An Overview of Hertz's Theory

The contact forces that arise during impact are due to the deformation near the contact area. This suggests that a more refined model which takes the geometric shape of each body into account may provide more accurate results for the system response during contact. In most cases, the geometric interaction is difficult if not impossible to describe mathematically, as the configuration may not be known *a priori*. However, in the special case of a spherical indenter, an approximate relationship is achievable using the well known Hertzian theory.

The contact force predicted by Hertz's theory is derived from the pressure distribution acting on the indenter during impact. The form of Hertz's law is well known and discussed at some length by Stronge [27], Chatterjee [5], Hunt and Crossley [10], Van Zeebroeck et al. [30], and Půst [20]. The elastic restoring force is given by

$$F = k_s x^{3/2}, \tag{31}$$

where k_s is a stiffness parameter for two colliding spheres is given as

$$k_s = \frac{4}{3} E_* R_*^{1/2} \quad . \tag{32}$$

The effective modulus, E_*, and effective radius, R_*, are related to the modulus of elasticity and radius of each spherical body by

$$E_* = \left[\left(1-\nu_B^2\right)E_B^{-1} + \left(1-\nu_{B'}^2\right)E_{B'}^{-1}\right]^{-1}, \qquad \text{and} \tag{33}$$

$$R_* = [R_B^{-1} + R_{B'}^{-1}]^{-1}. \tag{34}$$

Clearly, a spherical body impacting a flat wall is a special case of the above with $R_{B'} = \infty$, which implies that $R_* = R$, the radius of the pendulum mass.

Although the Hertzian model may seem restrictive because it only applies to spherical bodies, this model has the added benefit of being based on physical parameters instead of empirical values. The empirical values used thus far have the strong disadvantage that the experiment must first be conducted before the response can be predicted numerically. Using Hertz's model, the system response can be predicted based solely on published values for the modulus of elasticity, E_B, and Poisson's ratio, ν_B.

Hertz's Theory with Damping

The relationships described above have the advantage of being based on measurable material properties but also predict a perfectly elastic collision, i.e., an equivalent coefficient of restitution of $r = 1$. Simon [25] suggested a hybrid model obtained by modifying Hertz's equation to include viscoelastic effects by introducing a nonlinear damping term as

$$F = -k_s\,|\,x\,|^{1/2}\,(x + c\,|\,x\,|\,\dot{x}), \qquad \dot{x}(0) = v_0 < 0\,. \tag{35}$$

Following the presentation by Stronge [27], Hertz's model with nonlinear damping gives an equivalent coefficient of restitution that is velocity dependent and closely related to the discrete compliance model as one would expect. The differential equation is slightly different, given by

$$Z\frac{dZ}{dX} = \varsigma\,|\,X\,|^{3/2}\,(1-Z), \qquad \varsigma = \frac{kc^2R^{5/2}}{m} \tag{36}$$

obtained by making the substitutions

$$X = \frac{x}{R}, \qquad Z = c\dot{x}\,. \tag{37}$$

The expression (36) is integrated to obtain

$$Z - Z_0 + \ln\left(\frac{1-Z}{1-Z_0}\right) = \frac{2}{5}\varsigma\, X^{5/2}\,. \tag{38}$$

Evaluating (38) at the initial and final conditions, where $X = 0$, an expression identical to (30) is obtained,

$$\lambda(v_f - v_0) + \ln\left(\frac{1-\lambda v_f}{1-\lambda v_0}\right) = 0 \tag{39}$$

where $\lambda = c$. This implies that the relationship between the coefficient of restitution and impact velocity for the nonlinear lumped parameter model (Figure 3.5) is identical to the Hertzian model described by (35). Unfortunately, it follows that the model suffers from the same inability to correctly model the global system behavior. The results obtained were nearly identical to those shown in Figure 3.6.

Several more impact models using Hertz's contact force were investigated using the general form suggested by Půst and Peterka [20],

$$F(x,\dot{x}) = f(x)(1 + g(\dot{x}))\,. \tag{40}$$

The models investigated include $F = kx^{3/2}(1+\alpha\dot{x})$, $F = kx^{3/2}(1+\alpha\,|\,\dot{x}\,|\,\dot{x})$, $F = kx^{3/2}(1+\alpha\sqrt{|\,\dot{x}\,|}\,\mathrm{sgn}\,\dot{x})$, and $F = kx^{3/2}(1+\alpha\dot{x}^{3/2})$. Each of these models predicts a coefficient of restitution that decreases with increasing impact velocity but was still ineffective for modeling the current experimental setup. The most successful model was found to be $F = kx^{3/2} + c\dot{x}$, which produces a nearly linear relationship between impact

velocity and equivalent coefficient of restitution. Simulation results using this model are shown in Figure 3.7.

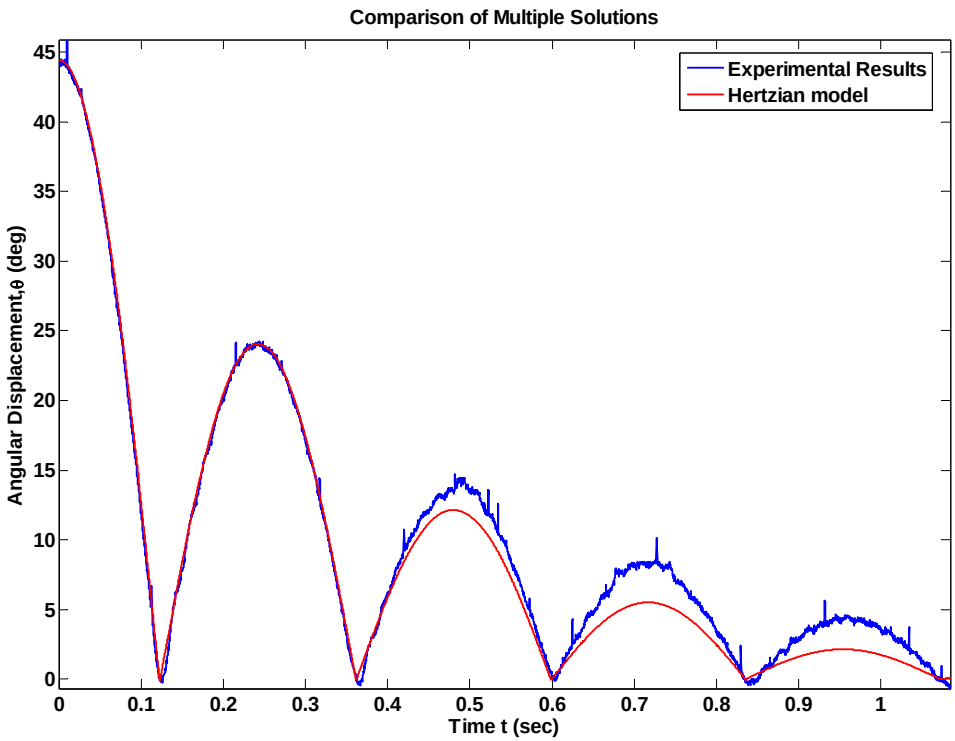

Figure 3.7: Comparison of experimental results with damped Hertzian model (E = 0.025426 GPa, c = 23 Nm/sec)

The modulus of elasticity was determined for the test material in a separate experimental nanoindenting procedure [13]. The damping coefficient was chosen by trial and error. Although the results match well up to the second point of impact, the solution quickly starts to diverge from the experimental results. This limitation is again related to inability of the model to correctly characterize the relationship between the equivalent coefficient of restitution and impact velocity.

Synthesis of Modeling Results

Several conclusions can be drawn from the detailed discussions above. The coefficient of restitution is a popular model due to the simplicity and ability to predict

global system behavior. For a small range of impacting velocities, the coefficient of restitution remains nearly constant. The range of velocities for which the constant value assumption holds is dependent on the material properties of the bodies colliding, namely the degree of viscoelasticity.

Compliance models represent the next step in contact modeling and have the added benefit of predicting the force-displacement history. The Kelvin-Voight model is the simplest compliance model, consisting of a linear spring and dashpot combined in parallel. The linear character of the Kelvin-Voight models predicts a constant coefficient of restitution based on the damping coefficient. Thus, the linear compliance model is subject to the same viscoelastic constraints as the coefficient of restitution model.

Many nonlinear compliance models can be expressed in the form $F(x,\dot{x}) = f(x)(1+g(\dot{x}))$. The nonlinear compliance models investigated in this work and by many others predict an equivalent coefficient of restitution that decreases with increasing impact velocity, in accordance with viscoelastic theory. A special case of the nonlinear compliance model is Hertz's relationship, which is based on a known elliptical pressure distribution for spherical contact. In this case, the stiffness can be computed directly when certain material properties are known.

The material chosen for this investigation was selected to demonstrate viscoelastic properties. However, the degree of viscoelasticity of the test specimen is much less than required by the nonlinear models above. Therefore, the linear models provide a much better prediction of the global system behavior. It is also instructive to compare the models on a detailed level near the region of impact. Figure 3.8 shows comparisons for three selected models near impact. The results are very similar for each case.

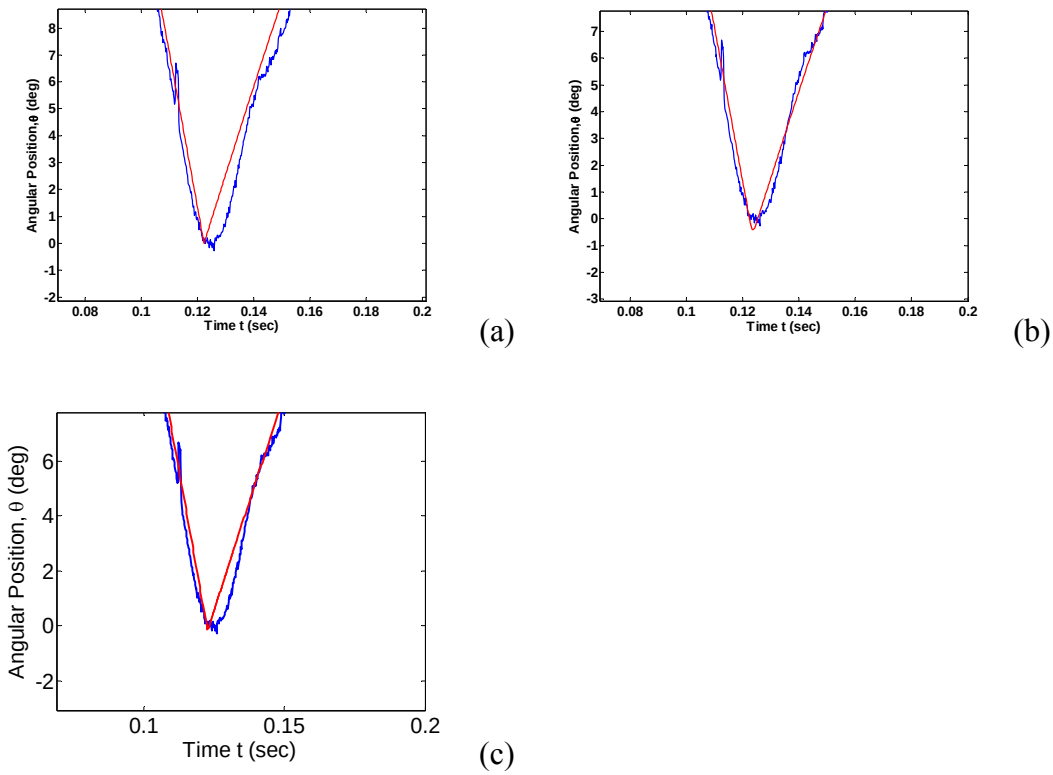

Figure 3.8: Comparison of contact model predictions near impact for (a) coefficient of restitution, (b) linear compliance, and (c) Hertzian with damping.

A New Linear Algebraic Contact Model

As noted previously, there are many different contact models existing for many different types of physical systems. However, none of the models considered to this point have accurately depicted the behavior of the experimental system under study. The linear models provided sufficiently accurate results, but failed to account for an important and identifiable trend, namely that the equivalent coefficient of restitution is a function of the linear impact velocity. The nonlinear models account for this relationship, but the results apply to a different class of materials than the test specimen chosen. It follows that the next step in the investigation should be to determine a model which accurately predicts the velocity-restitution relationship *and* applies to the material chosen.

Due to the lack of an existing model which accurately describes the experimental system considered here, a new model was developed. The model chosen predicts an equivalent coefficient of restitution that changes in a linear fashion as a function of the impact velocity. The equivalent coefficient of restitution is given as

$$r = r_0 - \alpha \,|\, v_0 \,| \tag{41}$$

where r_0 is the nominal coefficient of restitution. This model retains the simplicity demonstrated by the kinematic coefficient of restitution with the flexibility to account for a non-constant value over a wider range of impacting velocities. A relationship similar to this is reported by Hunt and Crossley [10] where $r_0 = 1$.

Expressing (41) in terms of the initial and final velocities at impact gives

$$v_f = v_0 (r_0 + \alpha v_0) \qquad v_0 < 0 \,. \tag{42}$$

For the limiting case of $v_0 = 0$, the equivalent coefficient of restitution model gives $v_f = 0$ as expected.

The expression for the coefficient of restitution (41) can easily be incorporated into the Kelvin-Voight linear compliance model by realizing that the damping parameter, γ, is a function only of the coefficient of restitution. From equation (21) it is straightforward to show that

$$\gamma = \frac{\ln(r)}{\sqrt{\pi^2 + \ln^2(r)}} \,, \tag{43}$$

which, using $r = r_0 - \alpha \,|\, v_0 \,|$, gives

$$\gamma = \frac{\ln(r_0 + \alpha v_0)}{\sqrt{\pi^2 + \ln^2(r_0 + \alpha v_0)}} \qquad v_0 < 0 \,. \tag{44}$$

Figure 3.9 shows results obtained using numerical simulation for selected parameter values.

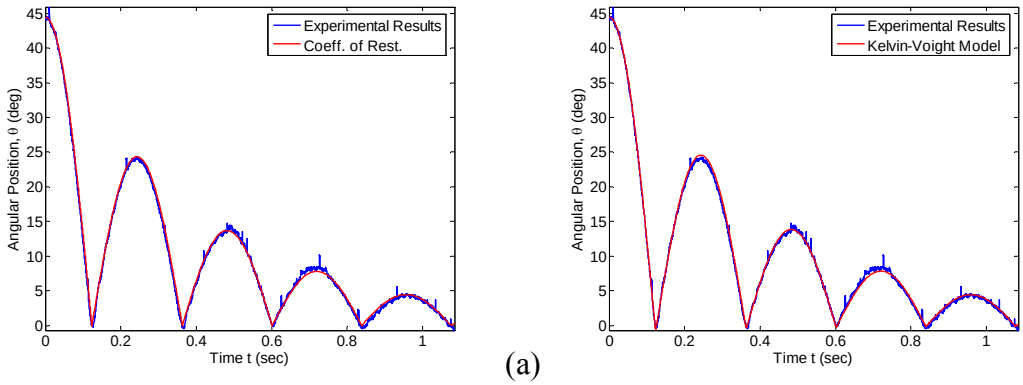

(a) (b)

Figure 3.9: Comparison of experimental and numerical results with (a) equivalent coefficient of restitution ($r_0 = .58, \alpha = .002$) and (b) modified Kelvin-Voight model ($r_0 = .58, \alpha = .015$).

The results compare well with experimental data in both cases. Although the above model is empirical, the flexibility allows the impact-restitution relationship to be accounted for. Furthermore, extending the model to the Kelvin-Voight representation allows the force-displacement history to be predicted. The results for the unforced impacting pendulum are marginally improved, but the capability allows for more dramatic improvements in the forced pendulum experiment.

CHAPTER 4
INVESTIGATION OF PARAMETRICALLY EXCITED PENDULUM

Each of the contact models presented thus far has been used to predict the unforced transient response of the impacting pendulum. The parameters which characterize these contact models were in many cases derived from the related experimental time series. The objective of this chapter is to extend the results previously obtained to further investigate the ability of the individual contact models to predict the complex motion of an impact oscillator. In accomplishing this, it has been assumed that the contact model parameters do not change between the unforced and forced experiments.

This investigation includes a presentation of the experimental results along with comparisons of numerical solutions using different contact models and further complexities regarding discontinuous dynamical systems are encountered. The results of a discrete frequency sweep are discussed and compared with numerical bifurcation predictions.

Several contact models have been incorporated into this work in order to show the effectiveness of different models in predicting the system response. This chapter seeks to broaden that investigation by applying the results to a more complicated situation. The three types of models considered were the kinematic coefficient of restitution, linear and nonlinear compliance models, and Hertz's model with linear and nonlinear damping. Further extensions were made by introducing a linear restitution expression that was a weak function of the impact velocity. From this selection of models, the coefficient of restitution and linear compliance models showed the most promising ability to predict the

dynamics of the current system, which was enhanced by the linear restitution relationship. Therefore, the objective of evaluating many different models has been achieved, and for the sake of brevity, only the coefficient of restitution and linear compliance model will be used for further investigations, employing the linear restitution relationship when necessary.

Many researchers have conducted detailed investigations of impacting systems demonstrating strongly nonlinear and chaotic behavior. Bishop has provided an overview of impacting systems and a survey of existing research [2]. A. B. Nordmark [18-19] has investigated the chaotic dynamics and grazing bifurcation phenomena associated with impacting systems. Bayly [1], Virgin [31], Moore [15], and Shaw [21-24] have contributed a great deal of work and knowledge to the study of discontinuous systems and related nonlinear behavior. Budd and Dux discussed chattering and related behavior [4]. This list is not exhaustive; the exciting and unexpected complexities associated with impacting systems have attracted the work of many others.

The objective of this section is to examine experimental data for the forced pendulum with motion constraints in place for a variety of frequencies and amplitudes and demonstrate the behavior similar to what has been shown already as well as some new and interesting dynamical features. The coefficient of restitution and linear compliance models will be used extensively in demonstrating the results. Important conclusions will be drawn regarding contact modeling for impacting systems.

Periodic and Complex Periodic Behavior

It is well established that linear systems respond to parametric excitation at the driving frequency where the amplitude and phase of the response are characteristics of the system damping and natural frequency. In nonlinear systems, this is not always true.

Nonlinear systems often exhibit harmonics, or response characteristics at frequencies that are rational multiples of the forcing frequency. Harmonics are usually identified by considering the power spectral density of a time series. Figure 4.1 shows the impacting pendulum response for a forcing amplitude of 4.6mm and a driving frequency of 4.2 Hz. The amplitude is horizontal displacement of the base and the driving frequency is the frequency at which the base oscillates. The response is computed using both the coefficient of restitution and linear compliance models, which are compared with experimental results. It is clear that the system response for this excitation is periodic.

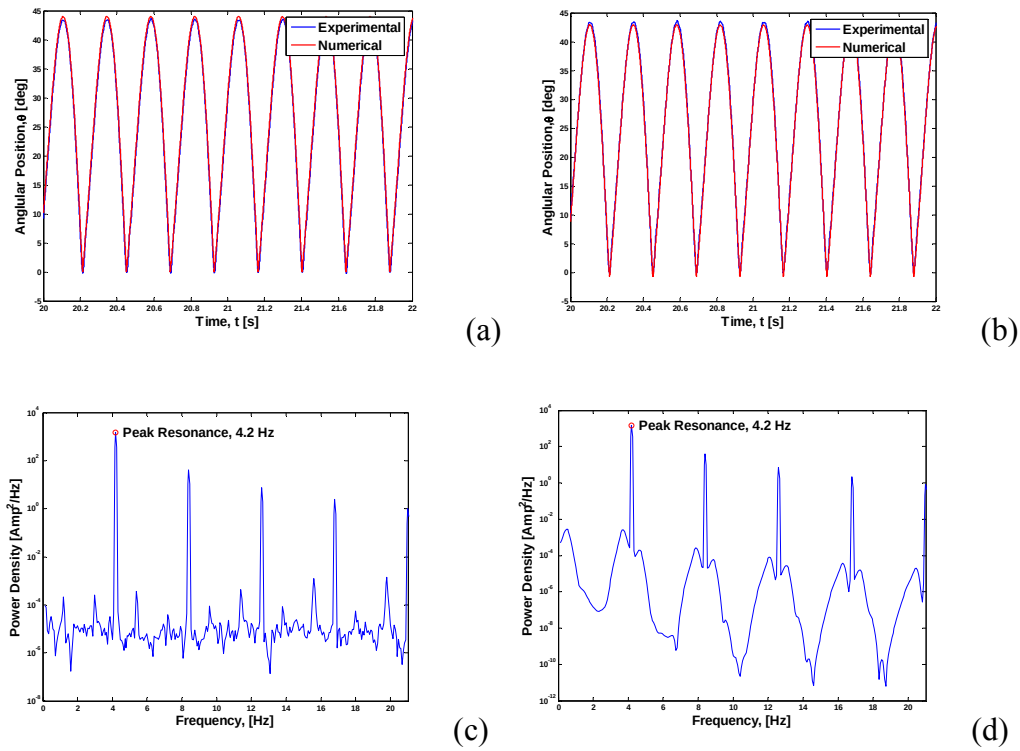

Figure 4.1: Comparison of experimental and numerical results for (a) coefficient of restitution (r = 0.6) and (b) linear compliance model (ω_0 = 723 rad/sec, γ = 0.14, r = 0.65) with A = 4.6mm and Ω = 26.4 rad/sec (4.2 Hz). Power Spectral Densities for (c) experimental and (d) simulated results.

Figure 4.1 (c) and (d) depicts the power spectral density (PSD) for the experimental and computational response, respectively. The peak response occurs at 4.2 Hz as expected. Harmonics are clearly shown at integer multiples of the driving frequency. The experimental and computational response and power spectral densities show excellent agreement.

Figure 4.2 depicts a response at 8 Hz closely related to the response at 4.2 Hz shown in Figure 4.1. The response is periodic as before, but the PSD indicates that the pendulum is responding at about 4 Hz, which is half of the excitation frequency of 8 Hz. The computational and experimental results compare extremely well.

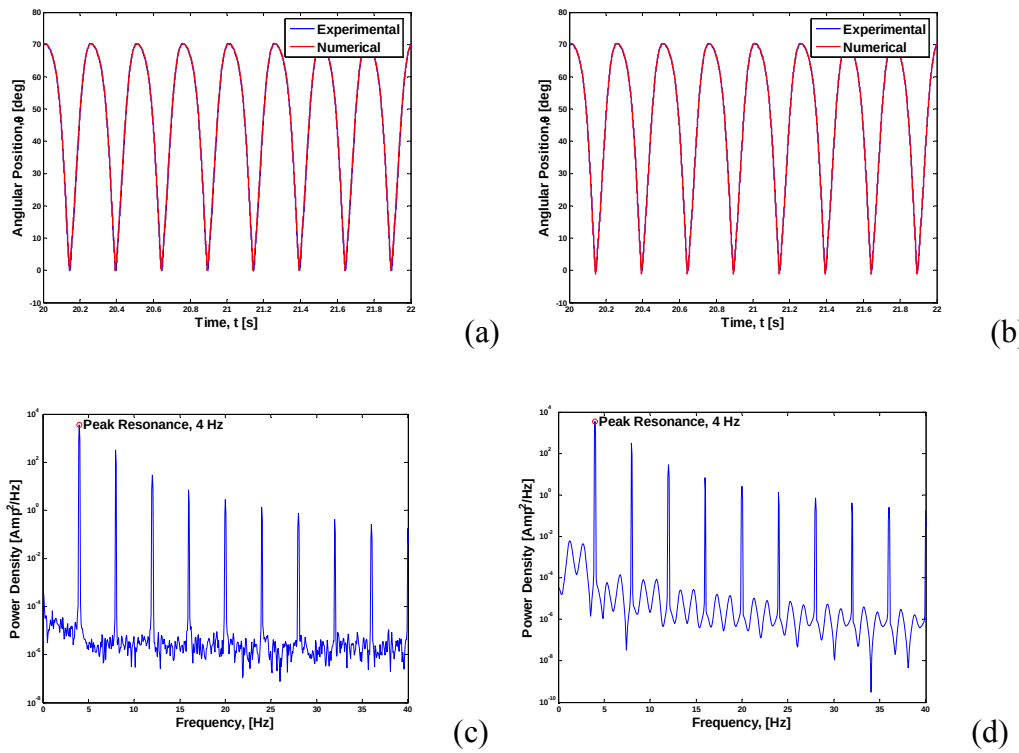

Figure 4.2: Comparison of experimental and numerical results for (a) coefficient of restitution (r = 0.6) and (b) linear compliance model (ω_0 = 725 rad/sec, γ = 0.165, r = 0.60) with A = 5.2 mm and Ω = 50.26 rad/sec (8 Hz). Power Spectral Densities for (c) experimental and (d) simulated results.

Figure 4.3 depicts further interesting nonlinear behavior which is complex periodic. In sub-figures (a)-(b), the computational responses predict periodic motion with a change of direction during free-flight. This behavior is confirmed with experimental data. Close inspection of the impact region also indicates a secondary impact of low velocity which results in a drastic rebound. This steady state behavior is sustained throughout the time series. Sub-figures (c) and (d) indicate that the primary response is at 3.73 Hz, approximately ¼ of the driving frequency of 15 Hz. The time series and PSD do not match as well as the previous periodic responses, but the agreement is impressive.

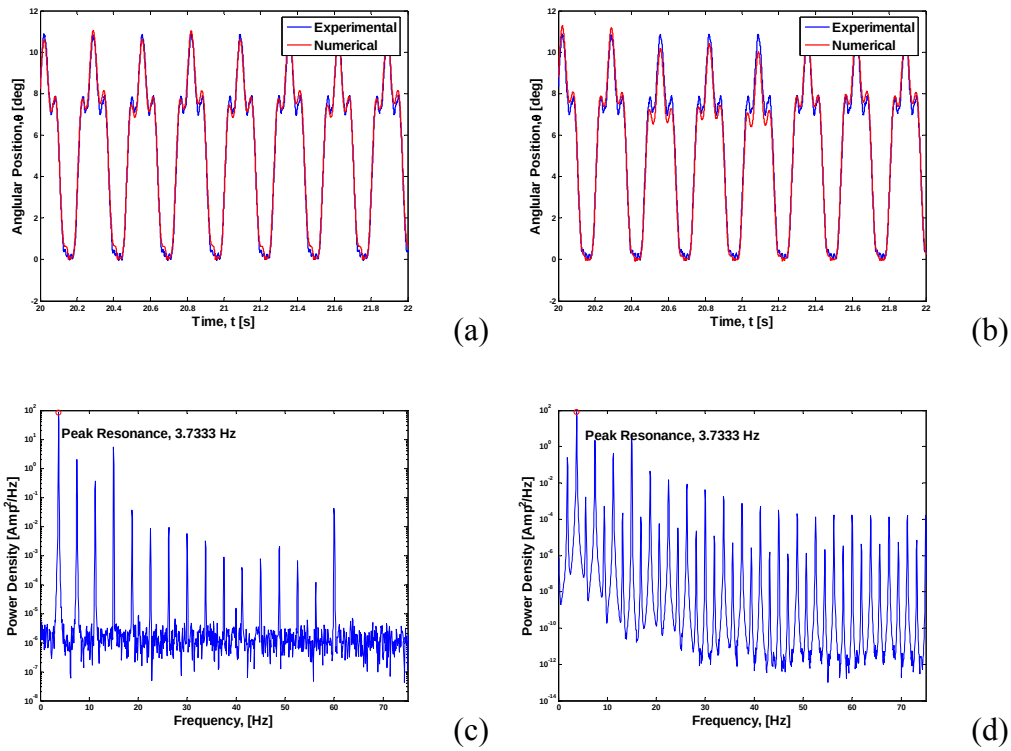

Figure 4.3: Comparison of experimental and numerical results for (a) coefficient of restitution ($r_0 = 0.6$, $\alpha = 0.05$) and (b) linear compliance model ($r_0 = 0.65$, $\alpha = 0.05$) with A = 1.0 mm and $\Omega = 94.25$rad/sec (15 Hz). Power Spectral Densities for (c) experimental and (d) simulated results.

Chattering, Sticking, and Chaotic Behavior

As previously noted, prior research of impacting systems has demonstrated a wide rage of interesting nonlinear behavior. One such phenomenon related to impact oscillators that has received surprisingly little attention in recent years is *chatter*[1]. C. Budd and F. Dux define chatter as a large or infinite number of impacts in a finite length of time, often leading to a similar behavior termed "sticking", in which the mass comes completely to rest on the impacting surface [4]. Budd and Dux investigate chatter for an idealized linear oscillator and develop means of predicting chatter and analyzing different basins of attraction leading to chatter. C. Toulemonde and C. Gontier also provide a detailed investigation of the sticking motion of impact oscillators [29]. Toulemonde and Gontier introduce methods for analyzing the stability, predicting the Poincare section, and determining bifurcations for chatter related behavior. The reader is referred to these works for a detailed presentation on the theory and analytical aspects of chatter and sticking behavior.

During this investigation, chattering and sticking behavior were discovered at low forcing frequencies. Each of the relatively few works that have been published is based on analytical work only and examines idealized mathematical systems. To the author's knowledge, this is the first published example of chatter and sticking that has been observed in an actual experimental impact oscillator. For this reason, the topic deserves further development. Furthermore, this behavior offers significant insight into different contact models.

---

[1] A distinction is necessary here. *Chatter* is also a well-known and thoroughly researched topic in machining and tool development. The use of the nomenclature arises from similar dynamical features between the behavior discussed here and that common to machining, but the two are not identical.

It is suspected that chattering behavior has not been investigated for an experimental system because the majority of research regarding impact oscillators has centered on “hard” or metallic stops with large coefficients of restitution in order to avoid the complicating viscoelastic effects. The polymer material selected in this study has an equivalent coefficient of restitution significantly less than unity, and thus demonstrates behavior not typically encountered. This scenario demonstrates one of the objectives of this thesis, which is to explore contact models for more complicated dynamical systems in order to expose different types of nonlinear behavior and test the limits of existing theory.

Figure 4.3 indicates an observed experimental response that demonstrates chatter followed by a region of sticking. From subfigure (a), for an excitation of A = 3.32 mm and 1Hz, the experimental system repeatedly reached a rotational displacement of approximately 15° followed by a steady decay to zero displacement for a finite amount of time. During this time, the pendulum no longer impacted the rigid stop, but remained at rest as the entire assembly moved as one rigid body. After a short time period, the pendulum suddenly jumped back to a 15° displacement.

The numerical predictions related to the occurrence of chatter, shown in subfigures (a) and (b), are also of interest. The coefficient of restitution model actually predicts, after a short amount of transients, that the pendulum comes to rest and stays motionless on the rigid stop. The Kelvin-Voight model, which takes compliance into account, predicts the periodic motion to a surprising degree of accuracy. In the subsequent section it will be shown that the coefficient of restitution model repeatedly predicts chatter, or a “stick solution”, that does not occur in the experimental system. The ability of the

compliance model to accurately predict this behavior is a significant difference between the models.

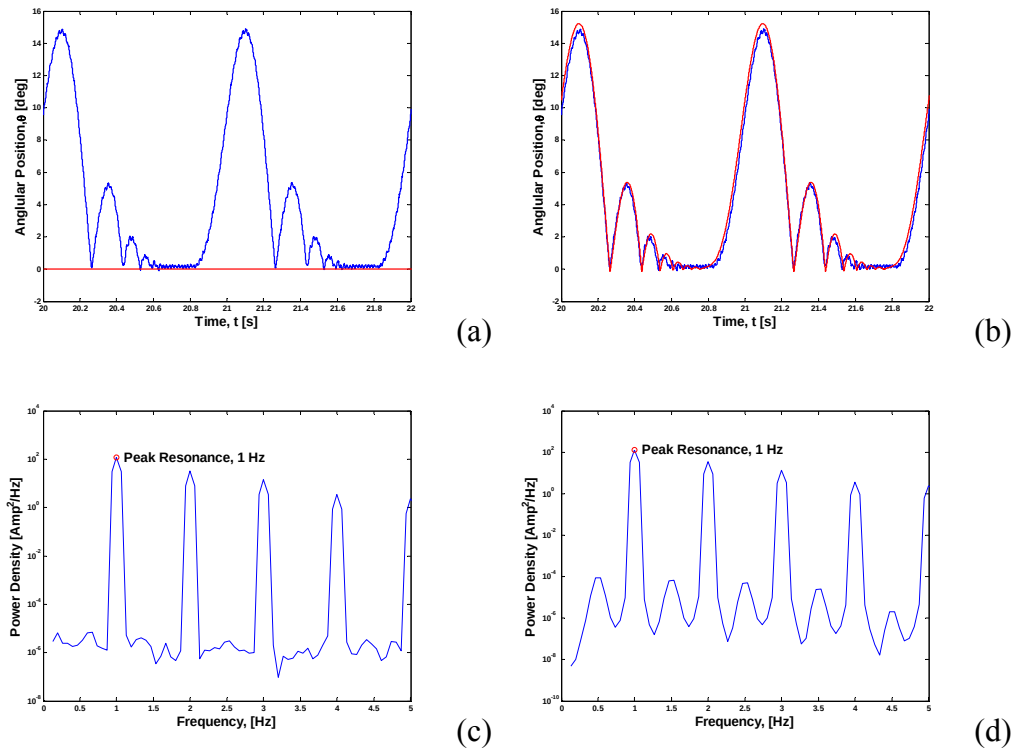

Figure 4.3: Comparison of experimental and numerical results for (a) coefficient of restitution ($r_0 = 0.6$, $\alpha = 0.05$) and (b) linear compliance model ($r_0 = 0.65$, $\alpha = 0.05$) with A = 3.32 mm and $\Omega = 6.28$ rad/sec (1 Hz). Power Spectral Densities for (c) experimental and (d) simulated results.

Figure 4.4 shows a clearer depiction of the simulated response using the linear compliance model. The red markers indicate the peak value during each inter-impact interval. It is apparent that the peak values rapidly approach zero and become nearly indistinguishable. Figure 4.5 shows the same response in the sticking region, indicating that the pendulum continues to penetrate the rigid stop during sticking. Figure 4.6 depicts the criteria which causes a subsequent rise after a short period of sticking. It is clear that the mass remains at rest (or nearly so) relative to the rigid stop until the

tendency of the acceleration becomes positive. At this instant, the mass begins the ascent away from the rigid stop, beginning the next period of motion.

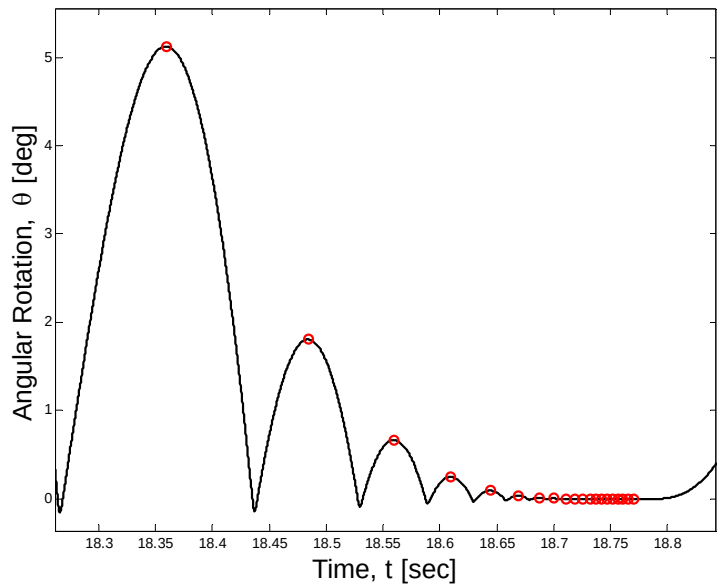

Figure 4.4: Simulated occurrence of chatter and sticking for A = 3.32 mm and Ω = 6.28 rad/sec (1 Hz). Red markers correspond to the peak value between each impact.

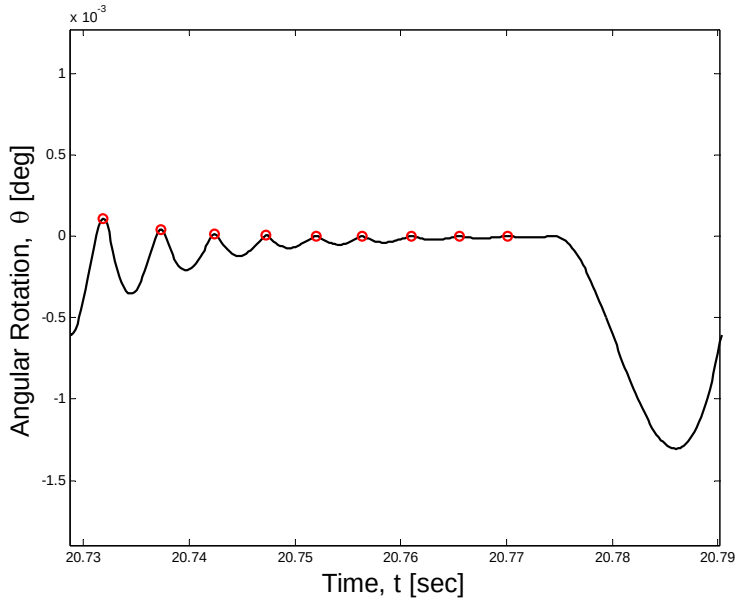

Figure 4.5: Simulated response during sticking for A = 3.32 mm and Ω = 6.28 rad/sec (1 Hz). Red markers correspond to the peak value between each impact.

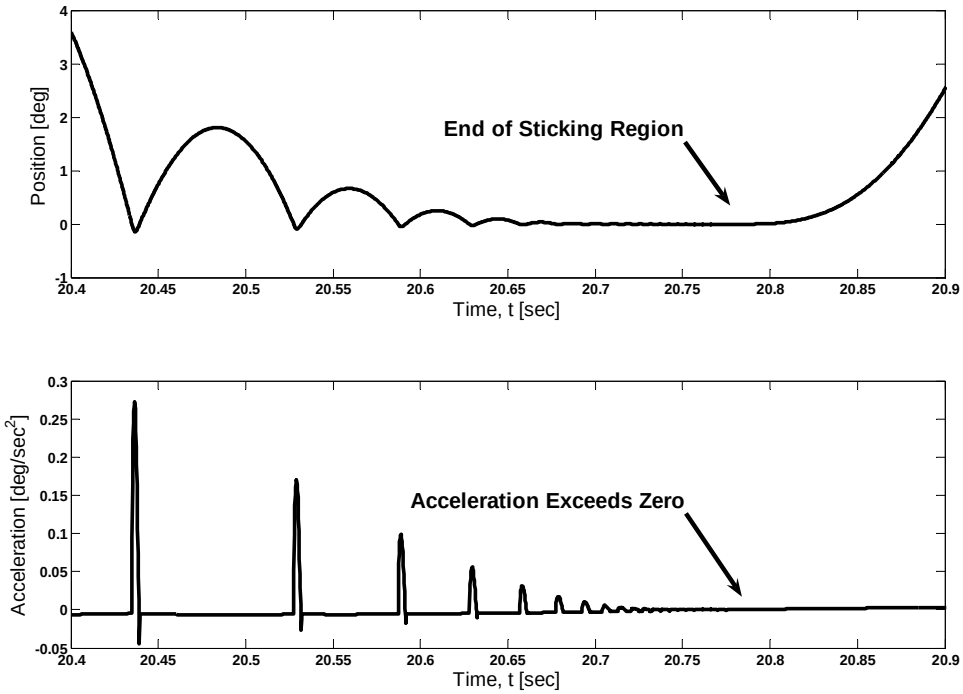

Figure 4.6: Comparison of chatter with acceleration for A = 3.32 mm and Ω = 6.28 rad/sec (1 Hz). The sticking region ends when the tendency of the acceleration (excluding sudden jumps above zero) becomes positive.

Chatter can be difficult to predict with simulation. In the exact case, chatter is seen as an infinite number of impacts in a finite length of time. Obviously, a numerical simulation is not capable of reproducing and infinite number of impacts and at some point will fail to predict future periodic motions. Figure 4.3(a) demonstrates this clearly. The coefficient of restitution model predicts that the system will reach a sticking region for the specified initial conditions and remain in that state, which is in effect a fixed point attractor for a nonautonomous system. The lumped parameter model, however, predicts that the system will never reach a *complete* state of rest, and eventually escapes the stable attractor at the origin.

Another interesting behavior that occurs only in strongly nonlinear, nonautonomous systems is chaos. Chaotic systems demonstrate a strong dependence on initial conditions and system parameters. For this reason, it is not plausible to expect a computational response to perfectly match a chaotic response over time, as it is impossible to perfectly estimate the system parameters and initial conditions for a given trajectory. Figure 4.4 shows a chaotic response at 10 Hz, in which the computational and experimental results are only qualitatively similar, as expected. The power spectral densities indicate that the signal has characteristics of broadband random noise, which is a well-known property of chaos. The coefficient of restitution and lumped parameter models are equally valid predictors of this complex response.

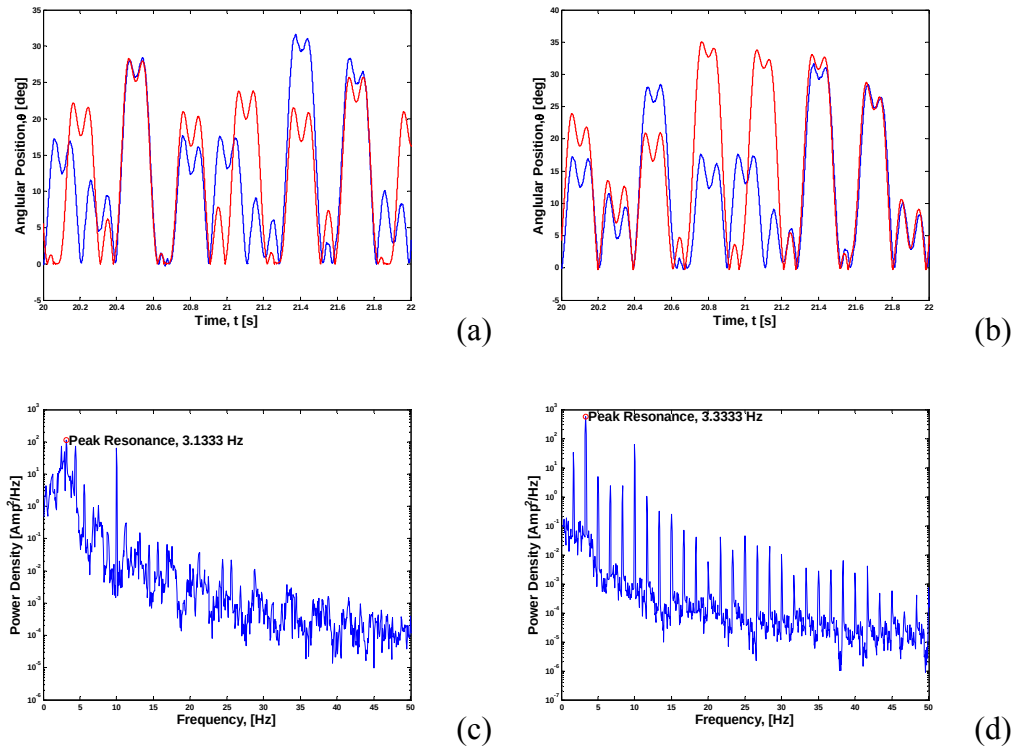

Figure 4.7: Comparison of experimental and numerical results for (a) coefficient of restitution ($r_0 = 0.6$, $\alpha = 0.05$) and (b) linear compliance model ($r_0 = 0.65$, $\alpha = 0.05$) with A = 3.1 mm and Ω = 62.8rad/sec (10 Hz). Power Spectral Densities for (c) experimental and (d) simulated results.

Bifurcation Diagrams

A *bifurcation* occurs in a nonlinear system when a static or quasi-static parameter change results in a drastic shift in the features of the dynamical response. One example is a stiff beam supported at both ends with a point load applied near the center. Increasing the applied load increases the deformation of the beam until a catastrophic bifurcation occurs, i.e. the beam fractures. Other systems may experience less dramatic bifurcations, such as a change in the stability of an attractor, as the system parameters are varied.

In order to determine the bifurcation points for the system under study, a discrete frequency sweep was conducted. Hardware limitations made a fixed amplitude frequency sweep difficult to achieve. As an alternative, a fixed voltage frequency sweep was carried out. This gave a forcing amplitude that decreased in an exponential fashion with increasing frequency, as shown in Figure 4.8. The computational frequency sweep was achieved by using a least squares regression equation to determine the amplitude at intermittent frequencies. The data were transformed using a base 10 logarithm to yield a curve accurately modeled by a polynomial. The regression equation was determined to be $\log_{10}(A) = -0.0004963\ x^3 + 0.019409\ x^2 - 0.33884\ x - 0.6252$, where the variable x is the forcing frequency in Hz.

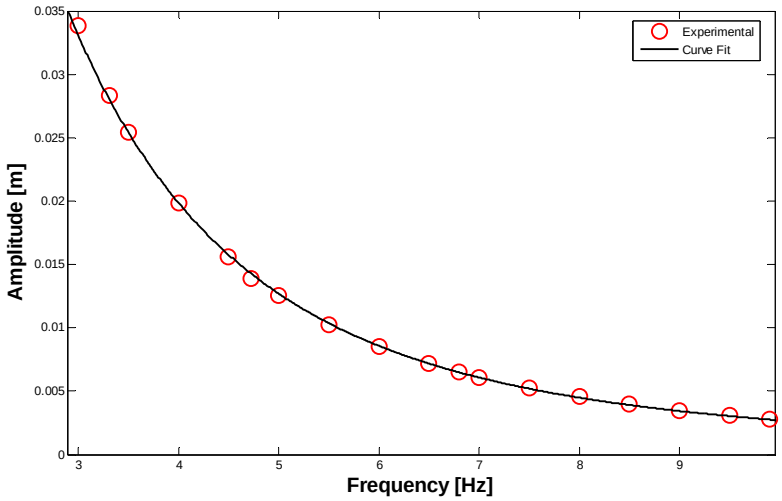

Figure 4.8: Relationship between forcing frequency and amplitude used for a discrete frequency sweep.

Figures 4.9 and 4.10 demonstrate the frequency sweep results using the coefficient of restitution and linear compliance models, respectively. The diagrams show very similar features, indicating that both models provide a good estimate of the system response. The exception is the occurrence of incomplete chatter, as shown by the blue markers in Figure 4.9. As demonstrated previously, the coefficient of restitution model predicts a fixed point solution when a stick solution is encountered. Exploratory work conducted by Budd [4] and Toulemonde [29] indicates that systems which experience chatter will often demonstrate *incomplete chatter*, a large number of impacts in a short time interval, near a chaotic attractor. Comparing Figures 4.9 and 4.10 indicates that most of the stick solutions predicted by the coefficient of restitution model appear in chaotic regimes, which supports the conclusions above.

A second feature which separates the two models is the appearance of parallel periodic solutions between 12 Hz and 14 Hz for the coefficient of restitution. This feature is not supported by experimental evidence. The linear compliance model

provides a better estimate for this frequency range, as shown in Figure 4.10. The false prediction shown in Figure 4.9 is suspected to be a limitation due to viscoelastic effects not accounted for by the instantaneous contact model.

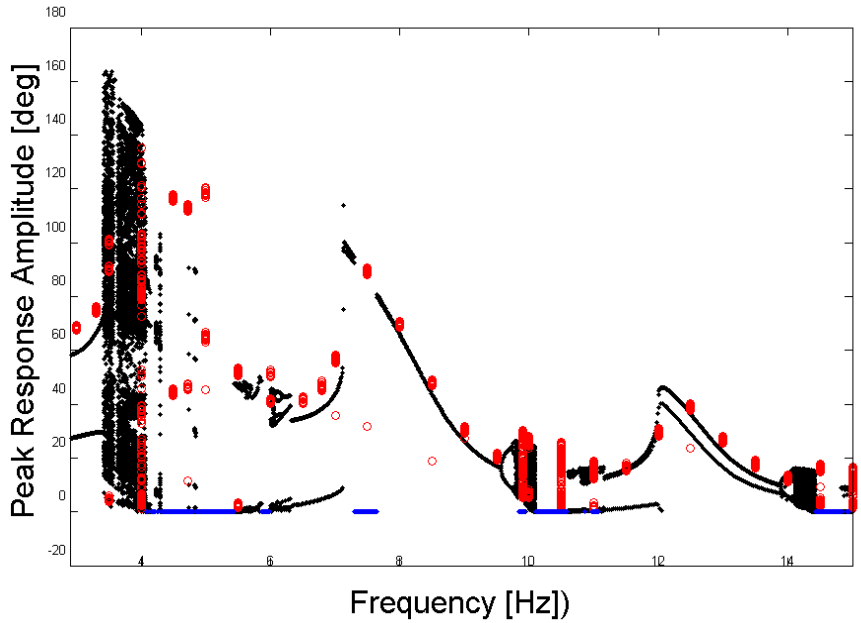

Figure 4.9: Bifurcation diagram using the coefficient of restitution (r = 0.6). Red is experimental, black is computational, blue is computational "stick solution" or chatter.

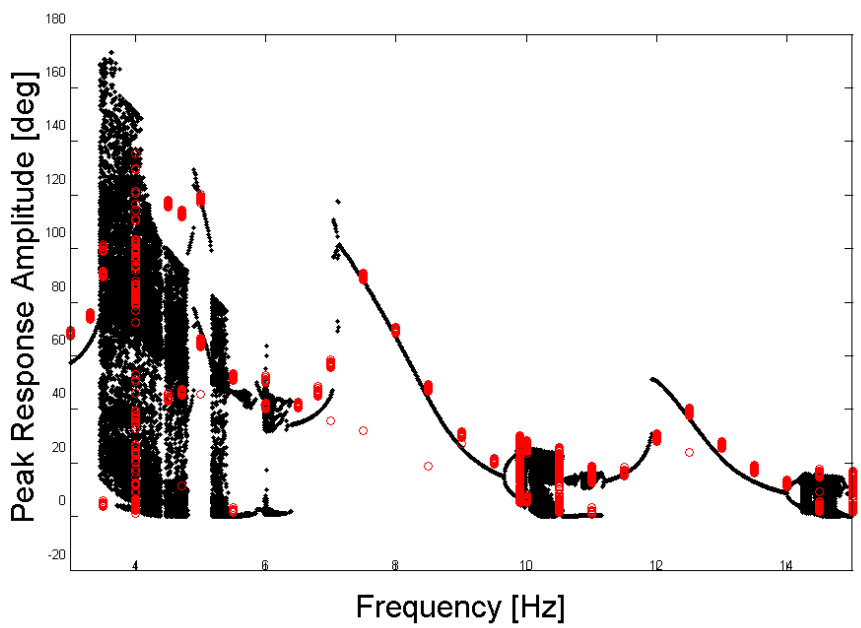

Figure 4.10: Bifurcation diagram using the linear compliance model (r = 0.6). Chattering is not predicted for driving frequencies higher than 3 Hz.

CHAPTER 5
CONCLUSIONS AND RECOMMENDATIONS

The objective of this thesis has been to detail an experimental and numerical investigation of a system undergoing impacts. Preliminary work discussed the classification, challenges, and analysis techniques for discontinuous dynamical systems and developed the analytical and computational tools necessary for further exploration of the dynamic system. The investigation included an overview of existing contact models, discussions of the relationships between these models, and selection of the models which best represented the actual system. A new algebraic relationship was introduced which enhanced the existing models and provided a better prediction capability for the system under study. Interesting nonlinear dynamics were demonstrated and investigated, including periodic behavior, period doubling bifurcations, and chaos. Chatter and sticking were demonstrated in the experimental impacting system and used to gain further understanding of the contact models. A discrete frequency sweep demonstrated the location of many types of nonlinear behavior and the bifurcation points separating these regimes.

The goal of this work was primarily experimental in nature, relying on existing theory as a foundation. Rather than attempt to introduce new concepts, prior research methods were surveyed and applied to a new type of problem to demonstrate the limits of the existing knowledge base, with the objective of enhancing the ability of scientists and engineers to account for more complex systems with a higher degree of fidelity. This was accomplished by selecting an impact material which is known to have viscoelastic

properties, and by using an indenter which experienced nonlinear free-flight behavior. Thus, the restrictions that other works have used to simplify results were removed in an effort to capture more of the underlying physics. This introduced further dynamical complexities, which allowed a more detailed investigation of the contact modeling and resulted in new types of nonlinear behavior being observed and accurately accounted for with simulation.

Although the objectives of the work were met successfully, several complications and limitations were encountered along the way. Perhaps the greatest limitation is the lack of a suitable compliance model for the type of material chosen for this investigation. Linear models such as the coefficient of restitution and Kelvin-Voight model, as well as nonlinear models, such as the Hertzian relationship, have been thoroughly researched in recent years. However, these models either apply to inviscid materials, where the equivalent coefficient of restitution remains constant, or to strongly viscoelastic materials, where the restitution relationship experiences an exponential decline with increasing impact velocity. The material used in this investigation had properties which both classes of models failed to describe accurately. As a result, an empirical approach was used to allow a weakly linear relationship between the coefficient of restitution and impact velocity. It would be preferable, in lieu of an empirical model, to develop a class of models which were equipped to accurately predict this in-between behavior.

Another major difficulty encountered was the inability to accurately estimate the contact parameters for the chosen models. It was shown that the energy dissipated during the impact of two bodies can be easily related to the large-scale motion after impact, which is easily measurable. However, the portion of the kinetic energy at incidence

which is transformed into potential energy elastically is completely recovered at separation. The result is that information about the impact must be known in order to determine the non-dissipative parameters. This suggests that a great deal of care should be taken in obtaining the proper instrumentation for measurement of the duration and/or penetration during contact when it is desirable to determine these model parameters. This would be the case, for instance, if it were desirable to know the force-displacement history during an impact to determine the unknown material properties or to predict certain changes in the behavior as a result of impact, such as the critical impact velocity which causes plastic deformation or excessive damage. Fortunately, the overall system response is largely unaffected by the elastic properties when the dissipative parameters are accurately characterized. This allowed sufficiently accurate results to be achieved with a minimal amount of information available.

In an attempt to cover a wide range of theory with applications to the current study, several important details were left unexplored. This is especially the case with the nonlinear behavior discussed in Chapter 4. Although several types of interesting behavior were demonstrated, the field of nonlinear dynamics is extremely rich with many intricacies which are still not yet understood. This experimental setup has different characteristics from the majority of systems in literature, which introduces the possibility of exploring and discovering new dynamical features and expanding the current state of the art. The discovery of chatter in the impacting system under study is proof that such behaviors do exist. Unfortunately, this type of analysis was outside the scope of this thesis, which has focused primarily on contact modeling, and only a limited amount of time was available for investigation into this exciting and rich field of dynamics.

Another possibility for future study is in the area of phase space reconstruction. Nonlinear time series analysis is often used to reconstruct the unknown states of the system when only a subset of states is known. Many tools have been developed, such as the false nearest neighbor test and the delayed embedding theorem, which allow the phase space to be reconstructed while preserving the topological and invariant features of the dynamics, such as the Lyapanov exponents. Some attempts have been made at applying these theorems and tools to discontinuous systems with initial success, but more development is needed. The area of phase-space reconstruction for discontinuous systems remains a largely unexplored field.

Extension of the ideas developed in this work to more complicated dynamical systems is straightforward. The methods developed for analysis of discontinuous dynamical systems apply to many forms of discontinuities, such as dry friction or stick-slip. Additionally, with the aid of a digital computer, the fundamental theory can be extended to simulate higher order systems with a large number of degrees of freedom. An intuitive grasp of the underlying physics dominating impact between two collinear rigid bodies is essential for successful application of existing theory to higher dimensional problems, and for the development of new theory.

In conclusion, this thesis has examined a specialized topic which, upon deeper understanding, may lead to further advances in science. It is hoped that this work will be a useful step in achieving the ultimate goals of understanding and solving real-world problems and applying engineering expertise to develop increasingly efficient and elegant mechanical systems.

LIST OF REFERENCES

[1] P. V. Bayly, K. N. Slade, L. N. Virgin, Extracting information from interimpact intervals in a mechanical oscillator. *Physical Review E* 56:3 (1997) 3705-3708.

[2] S. R. Bishop. Impact oscillators, *Philosophical Transactions: Physical Sciences and Engineering*. 347:1683 (1994) 347-351.

[3] B. Blazejczyk-Okolewska, K. Czolczynski, T. Kapitaniak, J. Wojewoda, Chaotic Mechanics in Systems with Impacts and Friction, World Scientific, Singapore, 1999.

[4] C. Budd, F. Dux, Chattering and related behaviour in impact oscillators. *Philosophical Transactions: Physical Sciences and Engineering*, 347:1683 (1994) 365-389.

[5] A. Chatterjee, Rigid body collisions: some general considerations, new collision laws, and some experimental data, PhD Thesis, Cornell University, 1997.

[6] S. Foale, S. R. Bishop, Dynamical complexities of forced impacting Systems. *Philosophical Transactions: Physical Sciences and Engineering*, 338:1651 (1992) 547-556.

[7] W. Goldsmith, Impact: the Theory and Physical Behaviour of Colliding Solids, Edward Arnold, London, 1960.

[8] M. H. Fredriksson, A. B. Nordmark, On normal form calculations in impact oscillators. *Proc. R. Soc. Lond. A*, 456 (2000) 315-329.

[9] M. Henon, On the numerical computation of Poincaré maps. *Physica 5D* (1982) 412-414.

[10] K. H. Hunt, F. R. E. Crossley, Coefficient of restitution interpreted as damping in vibro-impact. *Journal of Applied Mechanics*, 97 (1975) 440-445.

[11] D. W. Jordan, P. Smith, Nonlinear Ordinary Differential Equations. Oxford University Press, New York, 1999.

[12] M. A. Koplow, B. P. Mann, Bifurcations of a planar pendulum driven at a tilted angle. *2005 ASME Design Engineering Technical Conference*, Long Beach, September 24-28, 2005.

[13] B. P. Mann, O. Warren, G. Bourne, J.L. Tate, Experimental nonlinear identification in dynamic nanoindentation. *2005 ASME Design Engineering Technical Conference*, Long Beach, September 24-28, 2005.

[14] L. Meirovitch, Methods of Analytical Dynamics, Dover Publications, New York, 1998.

[15] D. B. Moore, S. W. Shaw, The experimental response of an impacting pendulum system. *Int. J. Non-Linear Mechanics*, 25:1 (1990) 1-16.

[16] A. H. Nayfeh, B. Balachandran, Applied Nonlinear Dynamics, John Wiley & Sons, New York, 1995.

[17] I. Newton, Mathematical Principals of Natural Philosophy and his System of the World (transl. by A. Motte; revised and annotated by F. Cajori, 1934), Univ. of California Press, Berkeley, 1687.

[18] A. B. Nordmark, Non-periodic motion caused by grazing incidence in an impact oscillator. *Journal of Sound and Vibration*, 145:2 (1991) 279-297.

[19] A. B. Nordmark, Existence of periodic orbits in grazing bifurcations of impacting mechanical oscillators. *Nonlinearity*, 14: (2001) 1517-1542.

[20] L. Půst, F. Peterka, Impact oscillator with Hertz's model of contact. *Meccanica*, 38 (2003) 99-114.

[21] S. W. Shaw, The dynamics of a harmonically excited system having rigid amplitude constraints, part 1: Subharmonic motions and local bifurcations. *Journal of Applied Mechanics*, 52(1985) 453-458.

[22] S. W. Shaw, The dynamics of a harmonically excited system having rigid amplitude constraints, part 2: Chaotic motions and global bifurcations. *Journal of Applied Mechanics*, 52 (1985) 459-464.

[23] S. W. Shaw, P. J. Holmes, A periodically forced piecewise linear oscillator. *Journal of Sound and Vibration*, 90:1 (1983) 129-155.

[24] D. W. Shaw, D. B. Moore, The experimental response of an impacting pendulum system. *International Journal of Nonlinear Mechanics*, 25:1 (1990) 1-16.

[25] R. Simon, Development of a mathematical tool for evaluating golf club performance, *ASME Design Engineering Congress*, 1967.

[26] A. Stensson, A. B. Nordmark, Experimental investigation of some consequences of low velocity impacts in the chaotic dynamics of a mechanical system. *Philosophical Transactions: Physical Sciences and Engineering*, 347:1683 (1994) 439-448.

[27] W. J. Stronge, Impact Mechanics, Cambridge University Press, Cambridge, 2000.

[28] J. M. T. Thompson, R. Ghaffari, Chaotic dynamics of an impact oscillator. *Physical Review A*, 27:3 (1983) 1741-1743.

[29] C. Toulemonde, C. Gontier, Sticking motions of impact oscillators. *Eur. J. Mech., A/Solids*, 17:2 (1998) 339-366.

[30] M. Van Zeebroeck, E. Tijskens, P. Van Liedekerke, V. Deli, J. De Baerdemaeker, H. Ramon, Determination of the dynamical behaviour of biological materials during impact using a pendulum device. *Journal of Sound and Vibration*, 266 (2003) 465-480.

[31] L. N. Virgin, P. V. Bayly, An experimental study of an impacting pendulum. *Journal of Sound and Vibration*, 164:2 (1993) 364-374.

[32] O.R. Walton, Granular solids flow project. Rept. UCID-20297-88-1, Lawrence Livermore National Laboratory, 1992.

[33] M. Wiercigroch, Mathematical models of mechanical systems with discontinuities, in: M. Wiercigroch, B. de Kraker (Ed.), *Applied Nonlinear Dynamics and Chaos of Mechanical Systems with Discontinuities*, World Scientific, Singapore, 2000, pp. 17-38.

BIOGRAPHICAL SKETCH

Ryan Carter was raised in Pearl River, Louisiana, before attending college at Faulkner University, a Christian school located in Montgomery, Alabama. During his two years as a mathematics major at Faulkner, he spent his summers in Honduras, Central America leading a mission effort to repair damaged houses and schools, as well as strengthen and encourage the local church. After two years of undergraduate work, he transferred to Auburn University and achieved a bachelor's degree in aerospace engineering, graduating magna cum laude in the spring of 2003. After graduation, he joined the PALACE ACQUIRE (PAQ) intern program to work with the United States Air Force SEEK EAGLE Office (AFSEO) as a Store Separation Engineer. Ryan is a proud husband devoted to his wife, Melanie, and three young boys, Ethan, Isaac, and Levi.